FEASIBILITY STUDY FOR A MULTIFEED IN THE 43GHz BAND

A. Orfei[1], P. Bolli[2], A. Cremonini[1], S. Mariotti[1], J. Monari[1],
V. Natale[1], R. Nesti[3], M. Poloni[1], A. Scalambra[1]

1 INAF-IRA, Istituto Nazionale di Astrofisica - Istituto di Radioastronomia
2 INAF-OAC, Istituto Nazionale di Astrofisica–Osservatorio Astronomico di Cagliari
3 INAF-OAA & MECSA, Istituto Nazionale di Astrofisica–Osservatorio Astrofisico di Arcetri-MECSA

Rapporto Interno IRA 400/07

Maggio 2007

D:\ProgettiInCorso\Faraday\progetto\Fattibilità43GHz\RapInt400-07_FeasibilityStudy40-50GHz.doc

PREFAZIONE

Il presente rapporto è stato prodotto nell'ambito del progetto finanziato dalla Comunità Europea chiamato FARADAY (Focal-plane Arrays for Radioastronomy, Design Access and Yield). Il progetto, iniziato nel novembre 2001 e originariamente della durata di tre anni, si è protratto con due successive "no cost extension" fino al dicembre 2006.
Questo studio di fattibilità era previsto come continuazione naturale dell'oggetto vero del progetto che, per ciò che concerne il sottoprogetto 2, assegnato all'IRA, riguardava originariamente la realizzazione di un ricevitore multifeed operante nella banda 21-26GHz (descritto in altre pubblicazioni).

INDEX

1. INTRODUCTION

2. SCIENTIFIC AIMS FOR USING MULTIFEED IN THE 35-50GHz OBSERVING BAND

3. RECEIVER ARCHITECTUREs AND FEEDs DENSITY
   3.1 Schemes for allowing multi purpose high sensitivity observations
   3.2 Optimization of the feed quantity

4. PASSIVE COMPONENTS STUDY
   4.1 Cryostat window
   4.2 Horn illumination for optimizing the G/T
   4.3 Circular vs Linear Polarization outputs

5. HIGH INTEGRATION FRONT END MODULE (HI-FEM)
   5.1 Introduction
   5.2 HI-FEM description
   5.3 Waveguide to LNA interface
   5.4 LNA
   5.5 Signal splitters
   5.6 Filters
   5.7 Post amplifier
   5.8 First conversion section
   5.9 Power supply

6. FREQUENCY CONVERSIONs IMPLEMENTATION FOR HIGH DENSITY MULTIFEED
   6.1 The problem of the huge amount of circuitry
   6.2 The injection of a noise calibrated signal into a huge amount of channels

7. MATTERS ARISING FROM VERY LARGE BANDWIDTH SYSTEMS
   7.1 Sensitivity depends on more than white noise
   7.2 Which components are responsible of 1/f noise value in a receiver chain
   7.3 Modulation techniques for overcoming 1/f noise
   7.4 Modulation techniques for overcoming Tsys fluctuations
   A7 Appendix to chapter 7

8. SENDING A LOT OF LARGE BANDWIDTH CHANNELS TO THE BACK-ENDs
   8.1 Overview of the data rates
   8.2 Fiber optic links for remoting signals

1. INTRODUCTION

The present feasibility study is due as deliverable in the framework of the FARADAY subproject 2 and originally called for a <<*...50-horn MMIC-based heterodyne arrays applicable to spectral line operation in the band 40 to 50GHz*>>.
The experience gained in yielding the main deliverable of the subproject <<*...a 5-horn criogenically-cooled heterodyne receiver array based on MMIC technology for spectral line dual polarisation in the band 21-26GHz...*>> allow us now to go further on those aims as well as we went in producing the 7-horn heterodyne receiver for spectral line and continuum in the band 18-26GHz. What we present in this report is a multifeed system capable of

a) observing not only for spectroscopy but for each astronomical observable,
b) exploiting the full receiver radiofrequency bandwidth. The bandwidth proposed here is larger than 40-50GHz and spans from 35 to 50GHz, making available for processing also the full 15GHz RF bandwidth so showing a *dual receiver in one,*
c) enlarging the use of MMIC technology till to propose an *all MMIC receiver*,
d) proposing an optimized dimension of the array. We show that the same observing efficiency of a 50-horn system could be obtained with less amount of horns properly oriented in the field of view of the antenna.

This study faces with all the relevant matters arising when a *very large bandwidth dense multifeed system* is placed under attention. They are

A) degree of integration of the electronics. This must be pushed at the extreme in order to avoid a huge amount of time in mounting and costing and thus requests a very high level of MMIC use,
B) optimization of the number of beams. This is for avoiding the cost inherent to the mechanical parts (feed systems, dewar and vacuum window dimensions): it could become not practicable for very dense multibeam,
C) receiver capability and data acquisition strategy for overcoming the receiver gain fluctuations. This aspect arises any time we face with large istantaneous bandwidth receivers,
D) find a simple and low cost solution for sending a huge amount of signals to the back-ends. The problem cost arises principally for the quantity of channels to be managed.

Some solutions can be described already now, some others, principally the development work in the field of the MMIC integration, are only sketched but with a confident degree of feasibility.

2. SCIENTIFIC AIMS FOR USING MULTIFEED IN THE 35-50GHz OBSERVING BAND

From a scientific point of view the availability of a receiving system in the 35 – 50 GHz band would open important observing opportunities in many fields of research, involving both spectroscopic and continuum (including polarisation) observing modes:

Examples for possible projects are:

I) Spectroscopy:

1) Molecular studies of star forming regions, circumstellar envelopes (CSEs), and comets.
   In the 35 – 50 GHz range the beam size of a 32-m antenna ranges between 50" and 70" and is thus suitable to map the molecular clouds in which stars are formed. Molecules that have transitions in this frequency range are NH_3, SiO, CH, H_2CO, CH_3OH, HCN, HCO^+, among many others, providing access to a range of temperatures and densities. In CSEs the important SiO maser at 43 GHz can be observed. Its emission originates closer to the stellar surface, with respect to the H_2O and OH masers, and thus provides important information on the current mass loss activity of the central star.
2) Search for new molecules in the Interstellar Medium and solar system objects.
3) Redshifted CO(1-0) emission of sources with redshift (z) between 1.3 and 2.3.
   The CO(1-0) rotational transition has a rest frequency of 115 GHz, which is shifted into the 30 to 50 GHz band for these values of z. CO is the most abundant molecule after H_2, and has therefore the highest chance to be detected of all molecules, as H_2 itself has no permanent dipole moment and cannot be observed at radio frequencies. Detection of CO in galaxy in this band allows one to determine its distance, and to get a (albeit very crude) estimate of its mass.

II) Continuum

1) Blind surveys of large areas of sky.
   A large-area sky survey at a frequency as high as 43 GHz may show a new source population which is different from the known cm-wave sources.
   Deep surveys at this frequency will also be essential for the upcoming Planck space mission as they would provide the high-angular-resolution information to the Planck large-sky surveys
2) Study of flat-spectrum radio sources (e.g. Flat-Spectrum Radio Quasars and BLLacs) or High-Frequency Peakers which are either often confused by `normal' steep spectrum sources at lower frequencies or much fainter due to absorption effects. In particular the High-Frequency Peakers are of vital interest as they are supposed to mark the earliest phase of radio galaxy evolution with typical source ages between 10 and 1000 years.
3) Follow-up of large surveys to study high-frequency spectra and polarisation properties of radio sources.
   Apart from the obvious astrophysical interests these observations will also enlarge the data base of suited calibration sources in this still relatively unexplored frequency range.
4) High-frequency mapping of extended sources
   The angular resolution of about 50" will allow mapping of extended sources (e.g. many radio galaxies, in particular giant radio galaxies) to reveal their morphology at an hitherto unreach frequency range.
5) The Sunyaev-Zel'dovich effect in galaxy clusters
   The expected decrease of brightness of the Cosmic Microwave Background radiation behind galaxy clusters provides a possibility both to find galaxy clusters at high redshift and to determine important parameters like masses or distances of already known ones.

III) High-frequency VLBI

It is obvious that many of the above-mentioned astronomical applications are also an issue for VLBI measurements. Adding another large station at frequencies around 43 GHz to the existing networks will mean an important improvement of the capabilities of the entire network.

3. RECEIVER ARCHITECTUREs AND FEEDs DENSITY

3.1 Schemes for allowing multi purpose high sensitivity observations

The new architecture receiver has as main goal the realization, in a single unit, of two different kinds of receiving system:

- the usual superheterodyne receiver allowing for *large bandwidth* though less than of the RF band
- an added receiver chain ables to exploit the full RF band allowed by the passive parts and LNA band design (*very large bandwidth*)

We propose for radioastronomy observations a new generation instrument by which pushing to an extreme the sensitivity due to the very large bandwidth available. In this case of a 7mm RF band we allow for 2 channels 2GHz wide outputs plus two channels up to 15GHz wide outputs for each beam.
The way to obtain this is sketched in Fig 3.1.1 and Fig 3.1.2. Both have pros and cons; in Fig. 3.1.1 the full RF outputs are branched before the first down conversion, in Fig. 3.1.2 this is obtained after the first conversion.
In the Fig. 3.1.1 solution, the RF Processing and Detection Unit can be both for Total Power and Polarimetry. The first one with 15GHz bandwidth, the second one with about 8GHz bandwidth because a correlator, made by passive devices, shows reasonable performance only in a relative band equal to about 20% of the central frequency.
Due to this reason in the solution 2 depicted in Fig. 3.1.2 the polarimetric facility is possible only with about 4GHz bandwidth since the central frequency value of the first conversion could be around 20GHz.
On the opposite, the solution 2 is more workable and cheaper because the circuitry is at a lower frequency range.

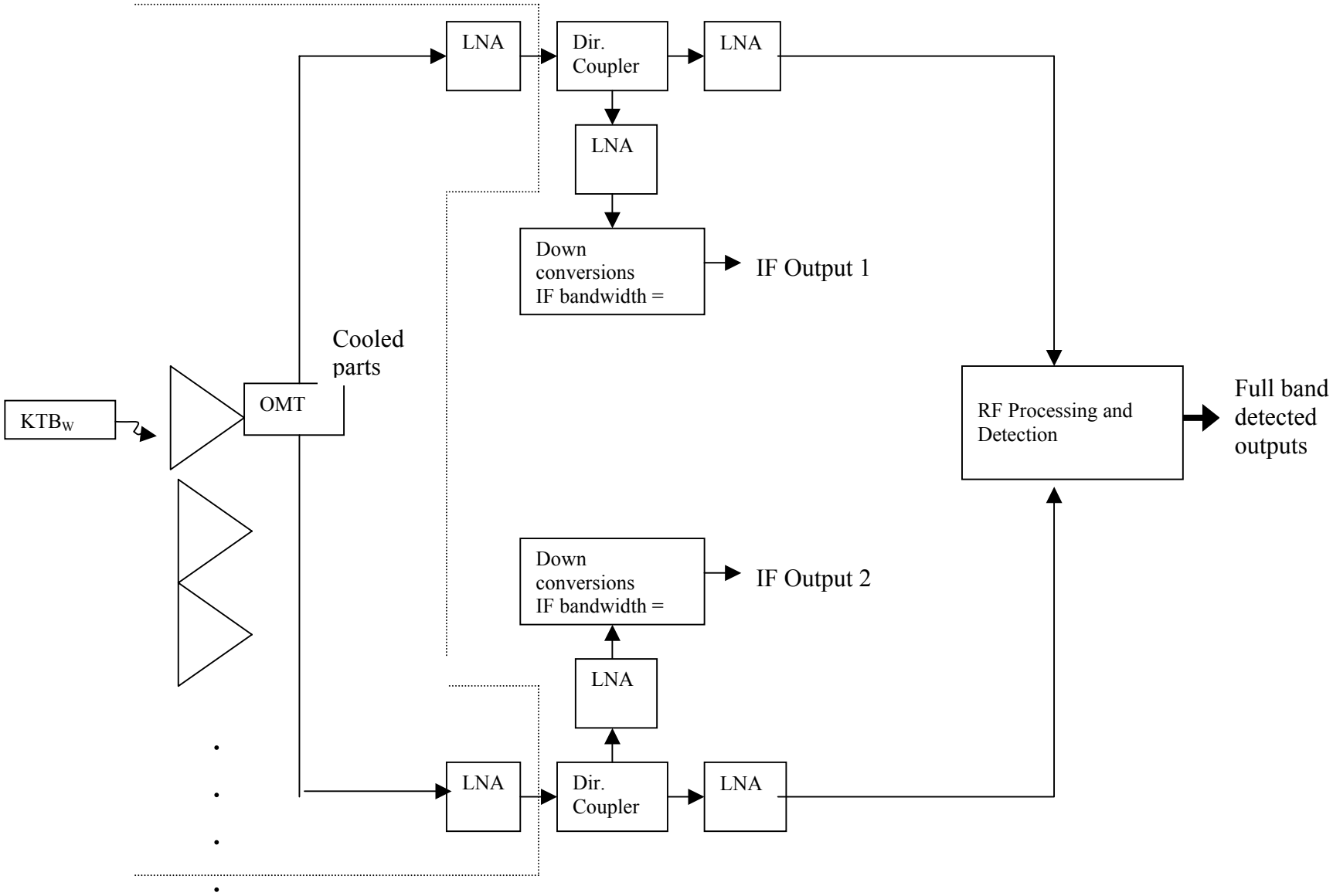

Fig. 3.1.1 Dual scheme *large* bandwidth *multifeed* receiver-solution 1

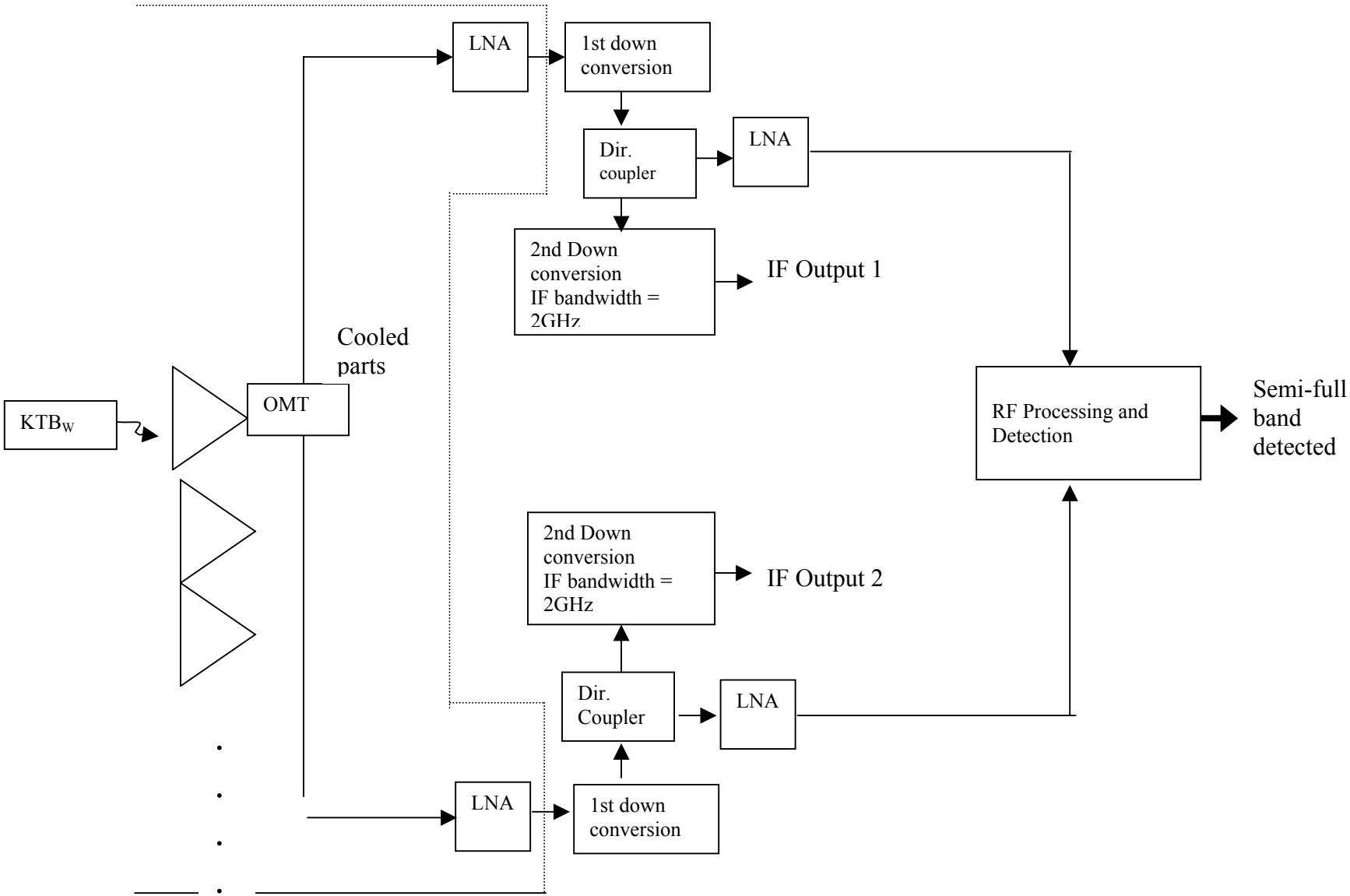

Fig. 3.1.2 Dual scheme *large* bandwidth *multifeed* receiver-solution 2

3.2 Optimization of the feed quantity

Currently, the rate at which astronomical information can be extracted from large dishes when observing spatially extended sources is limited by the use of single-beam receiver technology.
These receivers are approaching the fundamental limit sensitivity and the real observing sensitivity is limited by the atmospheric instabilities.
In the case of extended sources, maps of the source brightness distribution are made by moving the single beam in a regular fashion over the source. The rate at which data is acquired can be substantially increased by having multiple detectors in the focal plane of the telescope, each with a distinct beam on the sky. The potential gain in instrument productivity that can be realized by the deployment of multiple-beam receiver greatly exceed that which may come through other technological development in the near future.
Purpose of this work is to study the limit at which one can extend the array dimension for particular antenna and make a trade-off between the array dimensions and the technical difficulties in its implementation.

Focal plane sampling

Full sampling focal plane arrays have been demonstrated at 1.4 GHz [1] and at 6 GHz (Pharos preliminary tests). Current technology capabilities still prevent the use of this technique at higher frequencies.
Alternatively Position-Switch (PS), Raster-Scan (RS) and On-The-Fly (OTF) measurements are used. The relative efficiencies of these methods are deeply analyzed by Schieder & Kramer [2] using the Allan variance method.
In the following we assume the use of conventional corrugated feed horns as receiving elements arranged in square array at the focus of Medicina antenna whose relevant parameters are listed in the following Table 3.2.1.

Desctription	Symbol	Value[unit]
Primary diameter	D	32[m]
Equivalent focal length	f	97.311[m]
Magnification	m	9.485
Secondary inter focal distance	ds	10.0304[m]
Eccentricity	eps	1.23569
Equivalent f-number	F	3.04

Table 3.2.1

Furthermore we will focus our attention on OTF method. It can be shown that, to obtain a good coupling efficiency, the input radius *R* of the feed horn should be approximately

$$R = F*\lambda \qquad (3.2.1)$$

i.e. 3.04 wavelengths for the Medicina Cassegrain antenna, where λ is the wavelength and F is the f/D ratio in the focal plane.

For such a horn, using gaussian optics approximation, one can show [3] that the taper at telescope will be 9dB with a corresponding efficiency of about 0.8 and a FWHM of 1.142 λ/D ~ 45 arcsec @ λ = 7 mm (about 43 GHz).

The relevant horn parameters, for 40 GHz band, are:

Description	Symbol	Value[unit]
Horn aperture diameter	2R	6.1[λ] = 42.7[mm]
Edge taper phase error		1[rad]
Horn slant length	H	205[mm]

Table 3.2.2

To have a full sampling in the sky, the distance between the beams on the sky should be at least equal to the Nyquist rate of 0.5 λ/D. This limit translates in the focal plane to a distance d=0.5*λ∗F, hence in the optimum efficiency condition we have a minimum under sampling given by the ratio (2*λ∗F) / (0.5*λ∗F) = 4.

In practice, due to mechanical constraints imposed by the horn construction and physical dimensions of the passive front-end components (polarizer, OMT, ...) the horn inter-distance is larger than 2*λ∗F with a consequent under sampling factor larger than 4.
One can safely assume that it is possible to install the horns with an axis inter-distance

$$S = 2R + 10\text{mm} \sim 53\text{mm} = 2.5\ \frac{f}{D}\lambda \qquad (3.2.2)$$

So that the angular distance on the sky between two adjacent horn is

$$\theta = \frac{S}{f} = 113\text{arcsec} \qquad (3.2.3)$$

The actual under sampling, due to horn inter-distance, is then 5. Fig. 3.2.1 shows this condition for square arrangement where the horn positions are marked by circles and the position for Nyquist rate are marked by cross. To full sample the sky we need 25 telescope positions with PS method. Similar results can be obtained considering hexagonal geometry.

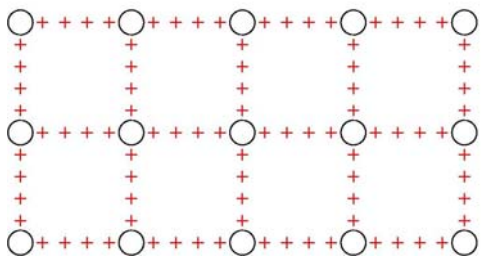

Fig. 3.2.1: Rectangular feed array arrangement (3x5 pixels)

Array dimension

The number of horn that can be accommodated in a focal plane strongly depend on the detailed antenna geometry. It can be shown that, at least in the limit of first order aberration, the best focus positions for off axis receivers, lie on a surface whose curvature (Petzval) is given by half the sum of the curvature of all the elements in the optical system. (Note. The first order aberration theory is not valid for shaped surfaces, as a consequence these results cannot be applied for example at the new coming Sardinia Radio Telescope (SRT)).

This is an exact result only in the hypothesis that the field curvature is the dominant aberration so that we can neglect spherical aberration, coma and astigmatism; in this last case the Petzval radius of curvature depends both on the radii of curvature of the focal tangential and sagittal surfaces .

Useful formulae for the aberration coefficients evaluation was given in [4] for large antennas.

A detailed study of the Medicina antenna focal plane has been carried out using both Zemax, an optical design program, and Grasp9 to verify the results in the microwave regime.

The optimization capabilities of Zemax have been used for receiver-to-subreflector distance search for the best focus by minimization of the wavefront error.

Field (degree)	d (mm)	Δ z (mm)	SR1	SR2
0	0	0	1	1
0.05	85.5	3.57	0.999	0.999
0.1	170.8	14.3	0.995	0.997
0.15	255.8	32.1	0.981	0.992
0.2	340.4	56.9	0.951	0.985
0.25	424.5	88.6	0.893	0.975
0.3	507.7	108.5	0.799	0.952

Table 3.2.3: Best focus positions as determined with Zemax

Table 3.2.3 shows the best focus position identified by d and Δz, respectively the distance from the optical axis of the antenna and the best focus position with respect to the geometrical focal plane toward the subreflector, versus the angular distance from the optical axis. SR1 and SR2 are respectively the Strehl Ratios before and after the optimization.

It is worth noting that, recalling the meaning of the Strehl ratio which can be approximated by the Ruze formula

$$SR \sim \exp(-(2\pi\sigma)^2) \qquad (3.2.4)$$

in the last entry of the table, the wavefront error is improved by about λ/13 to λ/28. However there is present a visible increase of the coma and astigmatism which cannot be corrected by shifting the horn on the Petzval surface.

Fig. 3.2.2 shows Δz versus d; one may note that, for not so large fields the dominant aberration is the field curvature with a Petzval curvature radius of 1137 mm.

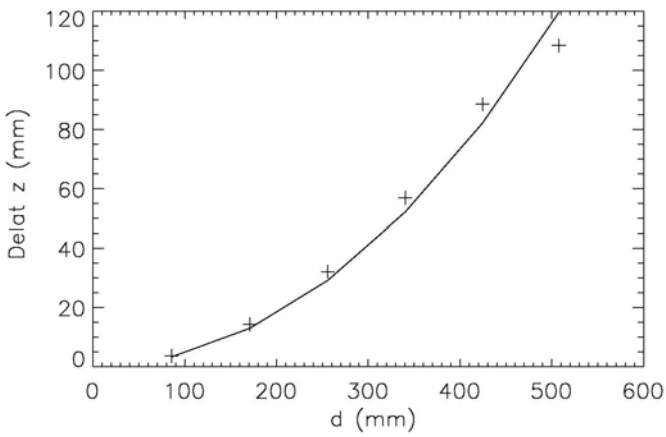

Fig 3.2.2. Position of the best focus versus the distance from the antenna optical axis.

A similar analysis has been performed through GRASP9, showing similar benefits due to the axial shift of the receiver. Table 3.2.4 shows for the same lateral displacements of Table 3.2.3, the antenna efficiency without (ε_an1) and with (ε_an2) the axial shift as determined with Zemax. It is important to point out that in the evaluation of the antenna efficiency, just the main contributions are taken into account: spill-over effects, taper illumination and secondary mirror blockage.

Table 3.2.4: Analogous results of Table 3 obtained by GRASP9

Field (degree)	d (mm)	ε_an1 [%]	ε _an2 [%]
0	0	78.3	78.3
0.05	85.5	78.0	78.2
0.1	170.8	77.0	77.2
0.15	255.8	75.0	75.8
0.2	340.4	71.5	74.0
0.25	424.5	66.2	71.6
0.3	507.7	58.8	68.8

Table 3.2.4: Analogous results of Table 3 obtained by GRASP9

Figure 3.2.3 summarizes the results reported in Tables 3 and 4. In this figure the curves of the normalized efficiency and Strehl ratio versus the feed lateral shift are plotted both with and without the axial displacement. The two analysis methods (GRASP9 and Zemax) implement different techniques and approximations yielding quite different results. However both the two analysis show that the recovered gain obtained exploiting the Petzval surface is very high: for example for the maximum lateral displacement (507.7mm), Zemax gives the 19% of overall efficiency and GRASP9 the 17%.

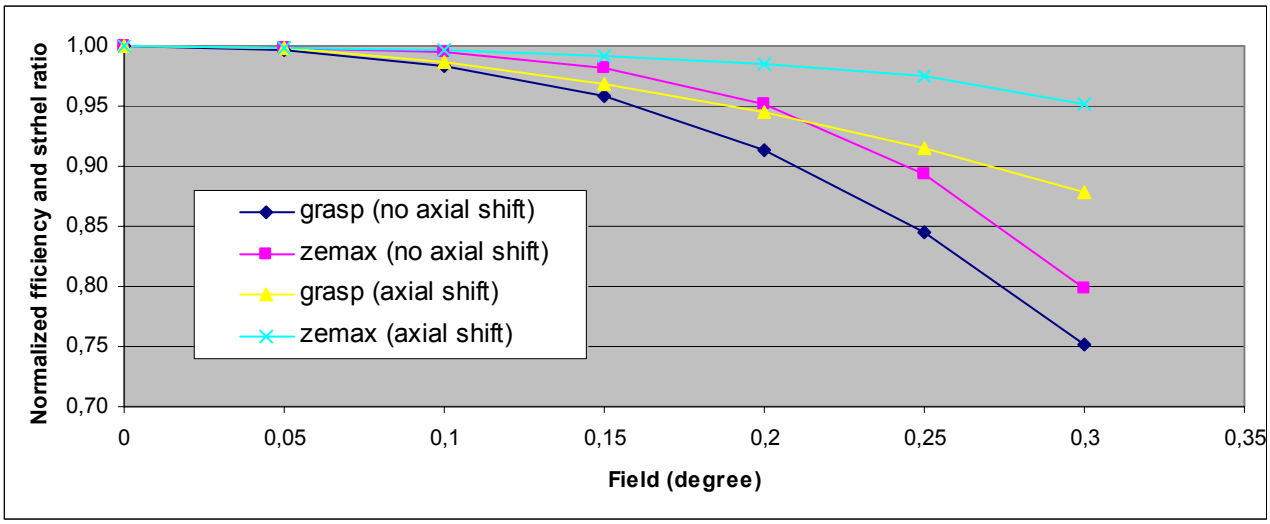

Fig. 3.2.3: Comparison of results between GRASP9 and ZEMAX

It would be possible to increase a little more the recovered gain by also tilting the feed, so to point its axis toward the primary reflector focus.

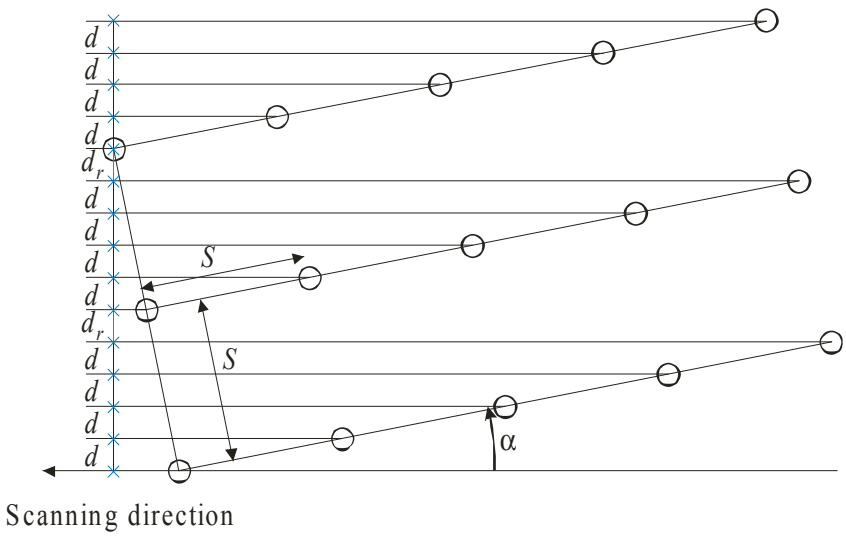

Fig. 3.2.4: Tilted rectangular array (3x5 pixels)

One of the option that can be used to fully sample the focal plane is the use of the OTF technique with a rotation of the array with respect the scanning direction.

Fig. 3.2.4 shows, as an example, a square array with a factor 5 of under sampling ($S = 2.5\,\frac{f}{D}\lambda$); to fully sample the sky it is possible to choose a minimum number $n = 5$ of elements in the scanning direction and a tilting angle α satisfying the relation:

$$d = S\sin(\alpha) \tag{3.2.5}$$

for elements on the same row and:

$$d_r = S\cos(\alpha) - (n-1)S\sin(\alpha) \tag{3.2.6}$$

for the end elements on two adjacent rows.

If it is imposed to have uniform spacing then $d = d_r$ leading to

$$S\sin(\alpha) = S\cos(\alpha) - (n-1)S\sin(\alpha) \Rightarrow \tan(\alpha) = \frac{1}{n} \Rightarrow \alpha = \tan^{-1}\left(\frac{1}{n}\right) = \tan^{-1}\left(\frac{1}{5}\right) \cong 11.31° \quad (3.2.7)$$

It is interesting to observe that by choosing the element number equal to the under sampling factor and imposing the uniform sampling spacing, the Nyquist rate in the focal plane is satisfied since we have:

$$d = d_r = S\sin(\alpha) < S\tan(\alpha) = \frac{S}{n} = 0.5\frac{f}{D}\lambda = N_r \quad (3.2.8)$$

Using this arrangement with the OTF technique, there is no advantage in an increase of the number of columns of the array, so we can state that, for a square array, the number of columns should be equal to the under sampling factor. The number of rows can be increased taking into account only the antenna field of view.
The instantaneous field of view can be freely increased increasing the number of rows. Similar considerations can be drawn for hexagonal arrays.

In our case, assuming a 5x5 array, we have an instantaneous field of view of 0.134^2 squared-degrees and an occupation in the focal plane of about 30^2 squared-wavelengths which imply a window diameter of about 430mm.
Finally, an increase of the instantaneous field of view for OTF can be readily obtained by increasing the separation between the horns; however a careful trade-off must be carried out taking into account the increased complexity of the system and the dewar window diameter.

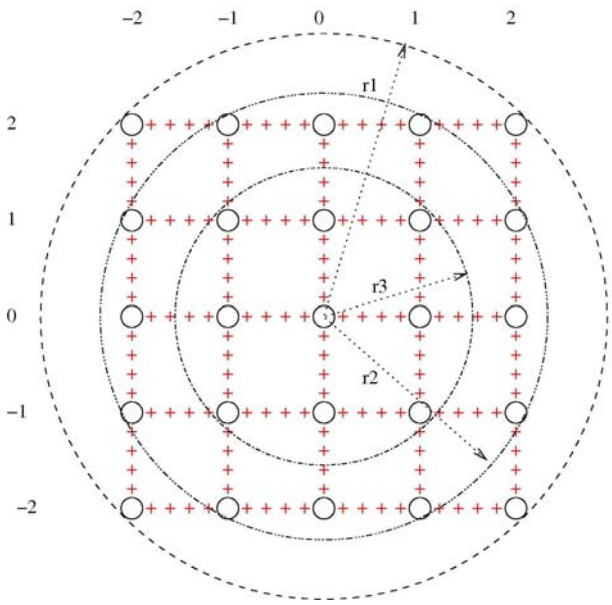

Fig. 3.2.5: Vacuum window diameter versus the array dimension.

Fig. 3.2.5 shows the window dimensions for three different array configurations, i.e. 5x5 full array, 3-5-5-5-3 and a 3x3 array; the corresponding window diameters, for the horn defined in Table 3.2.2, are
r1 ~ $2^{0.5}$*(2S+S/2) = 186 mm,
r2 ~ $[(2S+S/2)^2 + (S+S/2)^2]^{0.5}$ = 154 mm
r3 ~ $2^{0.5}$*(S+S/2)= 112 mm.
The problems arising from the use of large window (see next chapter) push toward compact arrays by the minimization of the horn input diameter and the consequent use of a suitable optics for the best coupling to the antenna.

REFERENCES

1. Fisher, Bradley
"Full-Sampling Focal Plane Arrays"
Imaging at Radio through Submillimeter Wavelengths, ASP Conference Proceedings, Vol. 217, edited by Jeffrey G. Mangum and Simon J. E. Radford, 2000
2. Schieder, Kramer
"Optimization of heterodyne observations using Allan variance measurements " A&A 2001
3. Goldsmith P.F.,
"Quasioptical systems"
IEEE Press 1997
4. R. Padman
"Optical Fundamentals for Array Feeds"
Astronomical Society of the Pacific Conference Series, Volume 75. Multi-Feed Systems for Radio Telescopes. Workshop held in Tucson, Arizona, May 16-18, 1994. Editors, Darrel T. Emerson John M. Payne, 1995

4. PASSIVE COMPONENTS STUDY

4.1 Cryostat window

Here we refer to the results sketched in Fig. 3.2.5
The thermal load on the cryogenerator due to the black body ambient emission is very high; for a 300mm windows the power entering into the dewar is about 32W. Some infrared filtering must be provided to limit to few Watts the thermal load while presenting a very low attenuation into the 35 - 50GHz band. An interesting filtering could be provided by a combination of a four Eccostock PP4 foils each 1.7mm thick plus a black polyethylene film 0.15mm thick installed on the 80K shield just behind the vacuum window.
This filtering will reduce the input thermal power to less than 10% with a radio frequency loss lower than about 0.1dB [1].

However there is a second drawback for relatively large window due to the material, normally Mylar, used for vacuum tightness. The window material generally exhibit relatively large dielectric constant (2.2 - 2.5); in order to introduce reflection losses lower than 1% it must have a thickness less than about $\frac{\lambda}{20}$ i.e. 0.3mm at 50GHz.
On the other hand thin films have increased permeability to atmospheric gases. For instance the Mylar [2] has the following permeability μ_P in units of $10^{-13}cm^3\,s^{-1}\,[cm^2/cm]^{-1}\,Pa^{-1}$.

Material	μ_P $[10^{-13}cm^3[cm^2/cm]^{-1}s^{-1}Pa^{-1}]$
Nitrogen	0.004
Oxygen	0.03
Water	100

Table 4.1.1

Considering a window having 0.1mm thickness and 300mm aperture diameter we have a ratio of film area/thickness equal to about $7x10^4$cm. Assuming a differential pressure (between room pressure and vacuum) of 10^5Pa we have an oxygen flux of

$$\dot{q} = 2.1x10^{-5}\,cm^3s^{-1} \qquad (4.1.1)$$

This relatively high flux will require the use of both active carbon and getters cryo pumping to guarantee long duration operation.

4.2 Horn illumination for optimizing the G/T

The feed horn for the frequency range 35 – 50 GHz is derived from the 18 –26 GHz design. A detailed study has been devoted to the optimization of the G/T ratio taking into account the overall dimensions of the horn. [3].
The geometry of the corrugations is given in Fig. 4.2.1. A curved profile for the horn has been chosen for the corrugations in order to achieve a structure as compact as possible and to have a very stable phase centre position in the frequency band.
The performances hav been optimised for return loss and for a cross-polarization maximum better than 30dB all over the bandwidth, as shown in Fig. 4.2.2.

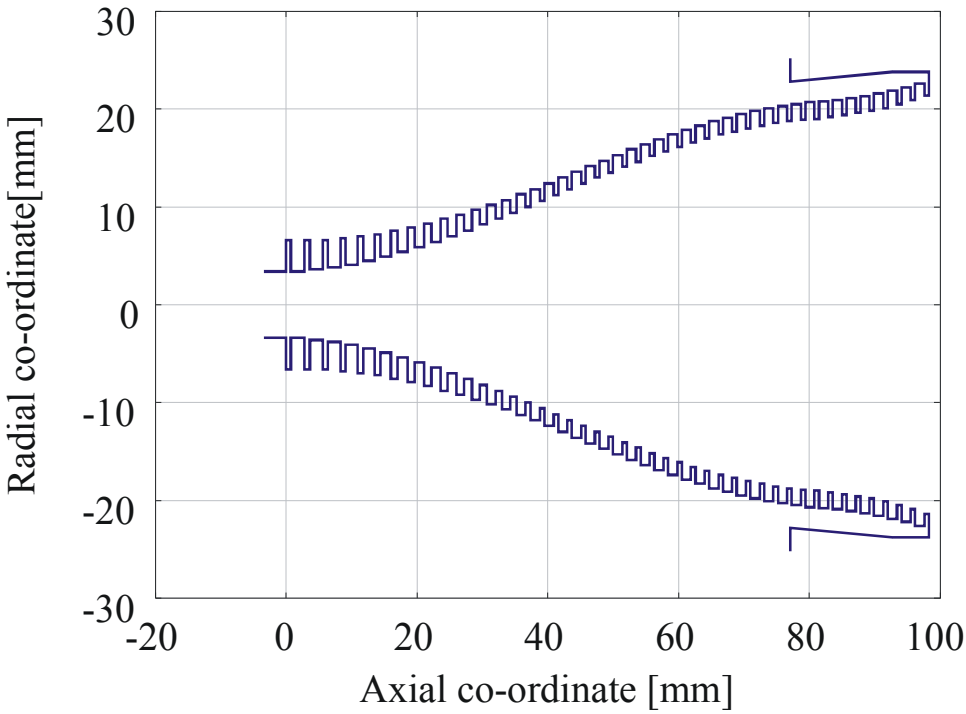

Fig. 4.2.1 Dimension of –9dB taper corrugated horn

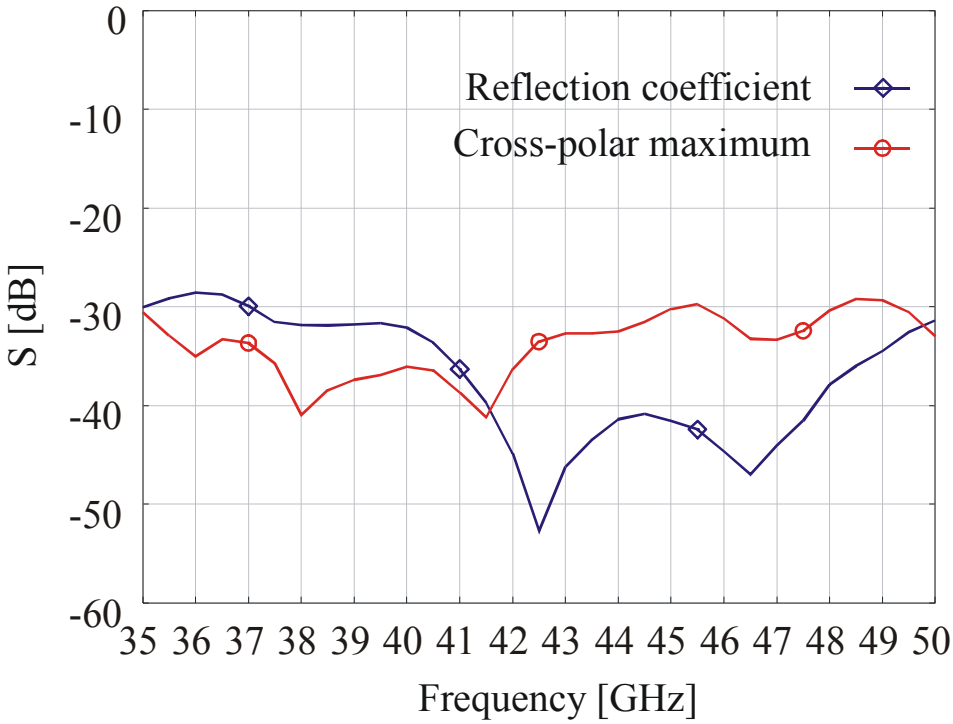

Fig. 4.2.2: Corrugated horn expected performances

4.3 Circular vs Linear Polarization outputs

This subject is important in order to avoid using polarizers, so space and weight could be saved into the dewar. This receiver anyway has to serve many different single-dish and VLBI observing programs. VLBI requires one beam but the use of circular polarization therefore at least the central feed should need a polarizer. Single-dish linear polarization measurements take a lot of advantage in using circular polarization. Possible alternatives can be either obtain the circular from the linear in the electronic chains using hybrid 180° or develop a polarizer/omt with dimensions such that

many of them can be allocated in a dense multifeed dewar. The following discussion assumes the need of a polarizer.

In those applications requiring information on the polarization state of the incoming signal a very good solution in this frequency band is a passive device placed in the receiver front-end. This device could be a polarizer or a simple Ortomode Transducer (OMT) in the case of, respectively, circular or linear polarization. Considering to extend at 43GHz the receiver developed at 22GHz, being the OMT the crucial part of the polarizer, for both mechanical criticalities and electrical performances, we focus here on the OMT itself.
The production of the septum turned out very difficult for the 22GHz OMT, since it must be placed inside the device with very high precision. Also the two circular bends of the side arms were critical at 22GHz, since their differential phase shift must be very low in order to avoid unacceptable performance degradation.
The new design at 43GHz has been done to overcome these problems (Fig. 4.3.1). A junction without a septum has been optimised: a multiple slot solution has been adopted doing the work of the septum and guaranteeing a better compromise between performances and mechanical criticalities at this frequency. Right angles and steps have been adopted instead of circular bends to recombine the side signal: this gives a shorter signal path in terms of the wavelength reducing differential phase problems.

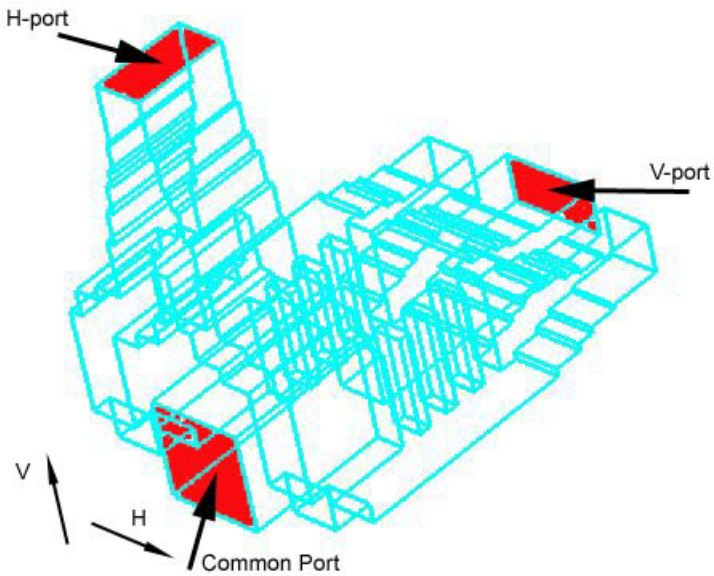

Fig. 4.3.1: New OMT design at 43GHz: electromagnetic model

Both solutions allow also to develop a compact structure, even more (in terms of the wavelength) of the 22GHz one; this feature is helpful in the view of Focal Plane Arrays (FPAs). The box envelope of the model shown in Fig. 4.3.1 has a side of about 25mm.
The performances of this design are given in Fig. 4.3.2 in terms of reflection coefficient of the two orthogonal polarizations at the Common Port.
The curves are related to simulation data. Two methods have been used, one is based on Time Domain (TD) and the other on Frequency Domain (FD). Although the methods are different the agreement is quite satisfactory in predicting a reflection coefficient far below –20dB for both the vertical (S_{11V}) and the horizontal (S_{11H}) polarization.

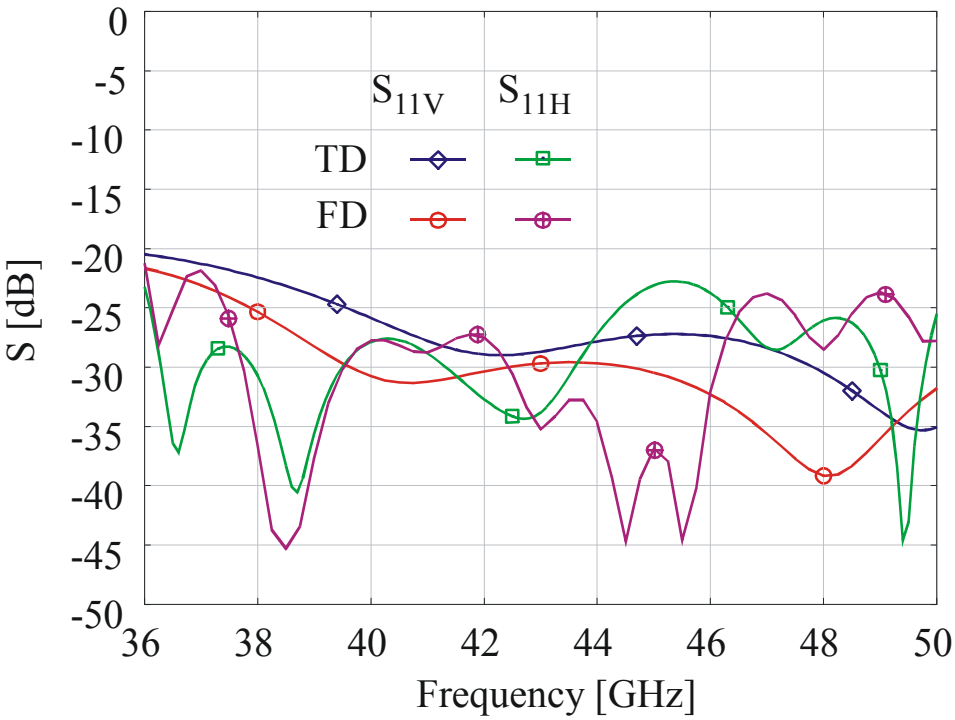

Fig. 4.3.2: New OMT design at 43GHz: performances

REFERENCES

1. Cresci,L., Natale, V., Panella, D., " Filtraggio della radiazione infrarossa nei ricevitori radio criogenici ", Unpublished report, 2006
2. http://www.goodfellow.com
3. R. Nesti
"Optimum feed taper value for the 18-26GHz multifeed system"
Internal report, april 2005

5. HIGH INTEGRATION FRONT END MODULE (HI-FEM)

5.1 Introduction

In an array receiver it is necessary to place a lot of components inside the cryostat. For this reason, wiring architecture and devices physical dimensions are critical points that must be carefully considered. To fit dozen of channels inside a cryostat the keyword is “integration”. In the following pages we will suggest solutions to realize a compact Front End Module (FEM). It is formally a Multi-Chip-Module (MCM) which includes, in a single carrier, several components commonly used in a receiver channel up to the first conversion. Moreover it will also provide a full bandwidth detected signal for total power observation purpose. In order to avoid unwanted EM propagations the carrier will be designed to provide individual caves for each function. When we cool down the devices, the related 1/f noise increase. In order to minimize this cooling side effect onto the receiver noise, we have to take carefully into account the components specification definitions.

HI-FEM specifications could be summarized in the following points:

- RF Waveguide Input (WR-22)
- Input Return Loss (IRL) better than -20 dB
- Embedded Noise generator for calibration purpose
- Direct Detected output
- Converted output down to 6-8 GHz (coaxial K connector)
- Lowest Noise
- High dynamic Range
- Overall Gain ≈ 45 dB
- Cryogenically coolable

5.2 HI-FEM description

In order to minimize the number of connections between elements inside the carrier and supported by the experience acquired during the FARADAY MMIC wafer runs, we will use MMIC (**M**onolithic **M**icrowave **I**ntegrated **C**ircuit) approach instead of MIC (**M**icrowave hybrid **I**ntegrated **C**ircuit) to design devices that will be placed inside the HI-FEM. Every function will be carried out by a specific MMIC realised with the best available foundry process. The Foundry process will be selected according to the function realised by the MMIC. In order to simplify the array receiver wiring architecture, bias distribution and noise calibrating signal will be provided inside the carrier. This solution will allow cost effective small mass-production and an extreme cryostat wiring simplification. Figure 5.2.1 shows a basically idea of how the HI-FEM could be composed.

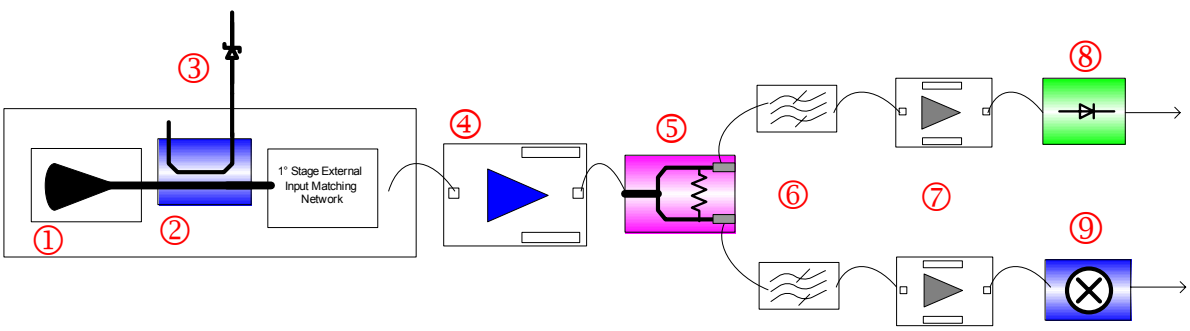

Fig. 5.2.1

1) WG to Microstrip transition.
2) Directional Coupler – Microstrip or Stripline
3) Noise Diode.
4) InP MMIC . Ultra LNA
5) MMIC Power splitter.
6) LTCC Filters
7) GaAs MMIC medium power amplifier .
8) Integrated Diode detector
9) Down Conversion (Mixer, Doubler, Buffer amplifiers)

1) Adapter will be an high performance, ultra low loss, wide band waveguide to microstrip transition.
2) Directional coupler will be carried out on a low loss microstrip substrate
3) Noise calibration signal have to be injected. Zener diodes still work at cryogenic temperatures, small and cheaper chip die exist on the market. Both sperimental and literature investigation are necessary in order to give trusted performances. Information regarding the noise power stability are very encouraging (<0.05dB/year). A control signal could activate or deactivate the noise generators very quickly (up to 1000 Hz or maybe faster).
4) Low Noise Amplifier (LNA) will be realised using InP MMIC foundry process. This technology has demonstrate to provide the lowest noise with an acceptable IRL and ORL. In order to reduce the noise, the first matching stage could be realised off-chip, on a low loss substrate. This approach is a trade off with a InP MIC LNA, realised using InP discrete active devices, discrete passive components and low loss substrate. InP MIC LNA could provide better noise performances but is not suitable for mass-production due to the higher cost and assembly time. Because the LNAs are cooled, ohmic losses are drastically reduced. This reduces also the gap between the technology, when we consider the receiver temperature system.

In order to reduce assembly costs and increase the yield we want realise the functions before the LNA on the same circuit, using low loss substrate like duroid or sapphire. This approach will allow more realistic electromagnetic simulation and will reduce packaging failure.

5) 0° Power splitter provide large bandwidth and is easy to fabricate on MMIC
6) If it will be necessary reject images and limit the RF bandwidth, band pass filters have to be used. Low Temperature Ceramic Cofired (LTCC) Technology must be investigated. It is possible realise high frequency broadband microstrip filters due to the narrow gap allowed by the technology.
7) Due to the very large bandwidth, non-linearities may occur. Post Amplifiers must provide gain, higher 1dB compression point and lower 1/f noise. These devices may be realised on GaAs HEMT or InGaAs mHEMT. These semiconductors intrinsically have higher noise (but noise excellence isn't requested at this stage) but are better power driven than InP. This solution increases the dynamic range of the receiver and the RFI receiver robustness.
8) The detector circuit, in a first stage, should be designed separately. In order to improve the integration, it could be included in the conversion and/or power splitter design, when the results are consolidated enough. The detector have to show low reflection coefficient and flat response. The diode is intended to detect the full RF band. In order to reduce 1/f contribution literature investigation will be necessary to choose the appropriate detector circuitry architecture. Experience aquired during the realisation of the BarSport radiometer, suggest a matched pair, zero bias detector.
9) The mixer will carry out the first RF conversion. It will provide high port isolation, low conversion loss and must be biasable in order to be tuned when placed in a cryogenic environment.

Front-End ports				
Power Supply	**RF IN**	**LO IN**	**IF OUT**	**Detected OUT**
+3V 0V –3V	35-50 GHz Waveguide WR22	TBD K-Coax.	6-8 GHz K-Coax	DC mV

Table 5.2.1

An alternative architecture, suitable to get lower drift is the following simplified Dicke receiver. The following architecture may permit both Dicke switching or Total power. The switch architecture may be carried out using MEMS or other Ultra low loss HEMT.

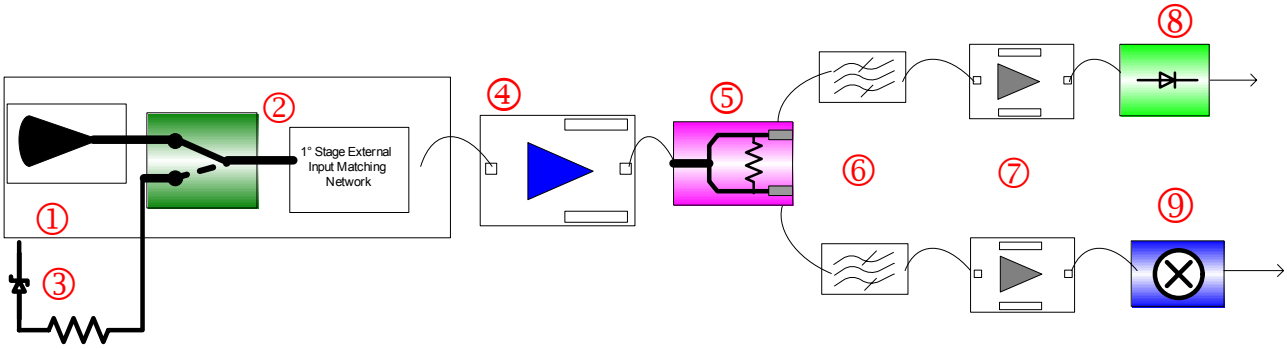

Fig. 5.2.2

1) WG to Microstrip transition.
2) Dicke Reference Load and Noise Source. When NS is OFF , it act as Dicke Receiver, When Switch is positioned to Resistance, by cycling ON-OFF the NS is possible to measure the Noise Temperature.
3) MEMS or (Ultra Low Loss FET) switch
4) InP MMIC . Ultra LNA
5) MMIC, 0° Splitter
6) LTCC Band pass filter
7) GaAs MMIC. LNA . Little bit higher Po1 and lower 1/F
8) Diode Detector
9) MMIC mixer.,MMIC Frequency Doubler and Power Amplifier

This second architecture could present more complexity and drawbacks than the first one. The switch introduce losses, and aren't easily predictable performances degradation after hours of switching. Then the repeatability of the switch stage condition isn't extremely clear. Maybe the application of a more efficient method of observation with the first receiver scheme, could provide the best trade off between architectures. A fast noise source ON-OFF switching will provide 1/f compensation with a simple scheme. This argument will be exhaustively discussed in a following chapter.

5.3 Waveguide to LNA interface

This circuit has to accomplish some functions, that are summarized by the following points:

- Convert the received EM waves to electric signal in order to be processed
- Provide a calibrating signal
- Include a low loss LNA Input Matching circuit in order to improve the Noise performances of the first amplifier

These functions have to be realised in a low loss media in order to reduce the attenuations before the first amplification stage. To satisfy the first specification a Waveguide to Microstrip adapter have to be designed. The design must consider bandwidth, matching, losses and mechanical complexity. Different solutions have to be evaluated in order to choose the best one for our

applications. Regarding the Noise Generator (NG), mostly single feed receiver architecture, it provides the calibrating signal using a diode, specifically designed for this purpose, connected with the RF channel by a directional coupler. The NG is commonly placed outside the cryostat and connected by a waveguide vacuum window and it serve only two channels. In a multifeed receiver, using switch or splitter to distribute the calibrating signal increase the wiring complexity inside the cryostat. Alternatively the calibrating signal could be radio injected through the horns, but this could increase mechanical complexity of the antenna system and the calibration time depends on the horn numbers. We suggest to integrated the NG into the HI-FEM. The overall system dimensions will be reduced, wiring architecture will be simplified and no vacuum windows nor waveguide lines are requested. In order to include the NG into a FEM, it will have to be validated in a cryogenic environment and a directional coupler must be designed as a component that injects the calibration signal into the RF channel. In order to keep losses al low as possible we are evaluating the possibility to design "off chip" the matching network of the LNA first stage. In order to design an optimum input matching network it is necessary to make an LNA MMIC Gopt characterisation.

Microstrip to waveguide transition for LNA input

In order to reduce the space occupation and masses inside dewar, because of high density of devices, a solutions to connect LNAs (designed in MMIC technology) with the feed system needs to be investigated. Moreover, the frequency range of interest, the Q-Band (33-50GHz), requires a particular connectors type. In the following table are shown the coaxial connector and the maximum working frequency.

Connector Type	maximum frequency
K	40 GHz
2.4mm	50 GHz
V	65 GHz
W1	110 GHz

Table 5.3.1

These types of connectors show several drawbacks, like cost, thermal load, space occupation mechanical weakness and RF losses. A solution is to design an input interface which will include a probe (a portion of microstrip circuit) which extends inside the waveguide on the broadwall. A typical situation could be represented in Fig. 5.3.1. With this solution the electromagnetic signal coming from the feed system could be coupled directly to the input microstrip circuit that will be wirebonded to the LNA. In order to match the input port a simple $\lambda/4$ adapter (impedance transformer) could be implemented or integrated into the LNA input matching circuit [1]. In-house design and fabrication capability are available up to 100 GHz for both E-plane and H-plane disposed radial launcher.

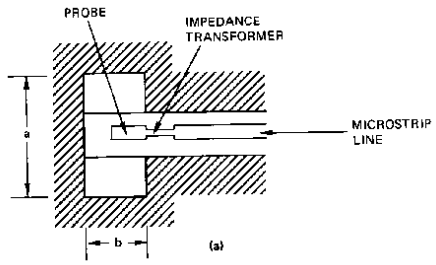

Fig. 5.3.1

5.4 LNA

This component has to provide enough gain to mask the rest of devices that follows down to the receiver chain, introducing less noise as possible. Indium Phosphide is the best proved technology for this application in a cryogenic environment, but also other technology like GaAs mHEMT or Indium Antimonide could be technologies that appear very interesting and theirs applications must be investigated. Encouraging results have been obtained with the second FARADAY InP MMIC wafer run at this frequency. The actual design could be improved in order to reduce the power consumption and reduce the 1/f noise. Modelling the InP device at cryogenic temperature will allow to optimize the LNA performances starting from the design.

5.5 Signal Splitter

Because the receiver will provide both direct detected and converted signal it is necessary to divide the RF chain. A 3dB Power splitter will be used. This component could be easily realised in MMIC.

5.6 Filters

If it should be necessary reject spurious signal, image frequencies or limit the RF bandwith to match the dynamic range of the detector, bandpass filters could be used. The maximum filters bandwidth could be 15 GHz, from 35 to 50 GHz. Wide bandwidth filters are usually provided in waveguide. Because our aim is to preserve a planar structure after the LNA, a microstrip or stripline filter could be the solution. Due to the high frequency and the wide bandwidth requested as specifications for this filter, process resolution specifications are too far for traditional microstrip filters realised in PTFE laminates. Low Temperature Cofired Ceramics (LTCC) will allow us to realise a planar or waveguided structure in a compact device, easy to connect and replace and providing the necessary bandwidth.

5.7 Post Amplifier

Function of this device is to provide gain with higher dynamic performance than LNA. Due to the intrinsic process characteristic, InP semiconductor offer the best noise performances but cannot give the same optimal result in term of power handling and gain drift. For this application GaAs HEMT or InGaAs mHEMT are promising better result.

5.8 First conversion Section

In order to be compatible with the system frequency mapping suggested for Sardinia Radio Telescopes (SRT) the first conversion LO has to sweep from 10.75 GHz to 13.5 GHz. This action will downconvert the RF signal to 6 to 8 GHz. These specifications are resumed in the following table

RF [GHz]		LO [GHz]		IF [GHz]	
		LO_L	LO_H	IF_L	IF_H
35	50	10.75	13.50	6.00	8.00

Table 5.8.1

The preferred technology to realize the MMIC mixer seems to be GaAs pHEMT or mHEMT process. Because this device will be cooled down to 20K should be biasable and passive in order to reduce power consumption and heat dissipation. Active mixer option which could provide conversion gain, could also be approached if this architecture will show better performances.

LO input.

While the LO distribution is conceptually simple, it's very expensive and often it sets a limit for the integration. Driving the LO's with coax cables rather than waveguides, will improve the integration capability. Also, driving LO at lower frequencies will reduce power losses along the line. It results convenient drive LO's at half of the frequency. A Power Amplifier (PA) and doubler will be placed between the LO distribution and the LO input of the MMIC mixer.

As we have described in the previous pages, HI-FEM require several different devices. For every function that could be carried out with a die-chip, there is an elected technology. The following table want to give a schematic view of the technological scenario around this module and the necessary efforts to realise it.

Function	Technology	Design Capability	Design tools
Switch	MEMS/HEMT	Never designed before. To be investigated device performances, complexity and design tools for the MEMS.	
LNA	InP MMIC	In house design capability and methodology. Could be interesting extract cryogenic models in order to design directly at 20K instead of design at 300K and make assumption at 20K.	EDA Linear Models
Post Amplifier	GaAs or InGaAs MMIC	In house design capability and methodology.	EDA Linear Models
Filters	LTCC	Never designed before. Medium complexity. There are at least two big companies which provide tools to design LTCC components. Time will be necessary to be in touch with the tools and the technology	Layout Marcos
Mixer	GaAs or InGaAs MMIC	High complexity. Never designed in house before. In Europe MMIC Foundry could provide GaAs models but at this working frequencies GaAs could provide worst performances than InGaAs. InGaAs mHEMT is a quite new unconsolidated industrial process, where InP devices are growth on a GaAs thick substrate. This technology can provide good noise performances and nice power handling capability. It must be investigated how this devices work in a cryogenic environment. Cryogenic models are unavailable and room temperature models provided by the foundry couldn't be so precise. Maybe models extraction in collaboration with Tor Vergata University could allow us to obtain the necessary models	Non linear models are necessary.

5.9 Power Supply

A reduction of the number of DC wires become necessary. We will study a supply solution, based on a temperature compensated voltage divider, which will work at room and cryogenic temperature.

It will be made by only 3 wires (+ for drains, return , and – for gates). A simple enclosed circuit will provide current regulation at all working temperatures. This solution may contrast 1/f noise, because the power supply currently adopted provide an Id stabilisation, which reduces the gain drift up to the 30%. The optimal solution will be to design a extremely compact customisable version of the existing NRAO power supply with a temperature follower included. Following investigation will be demonstrate if this way will be practicable.

REFERENCES

1. “Waveguide to Microstrip Transitions for Millimeter-Wave Applications”, IEEE MTT 1998

6. FREQUENCY CONVERSIONs IMPLEMENTATION FOR HIGH DENSITY MULTIFEED

One of the main problem for Multifeed systems is the available space for devices inside the dewar, the lack of space to keep electronics part close to the dewar, complexity, the amount of cabling and, of course, costs.

In order to reduce them, we are going to proceed with a standard two conversions super-heterodyne architecture (relative bandwidth <20% fc).
Following, we list point by point all the problems related to the different section thanks to the experience gained during the design and implementation of 22GHz Multifeed Faraday subproject 2.

6.1 The problem of the huge amount of circuitry

- First Conversion for frequency above 22GHz.
  We consider that the best solution is to have the mixer close to the LNA in order to avoid the RF cable and connector losses . For the highest frequencies is possible to study an hybrid LNA with the first mixer integrated.

- Power Supply for LNAs
  The development of power supply LNA boards allow to realize a sophisticated electronics and bias control. Unfortunately the cabling increase linearly with both the number of feeds and number of LNA stages. Same consideration is suitable for the vacuum connectors. So in order to reduce the costs, the cabling complexity and cooling losses, a bias solution that reduce dramatically the number of cables will be investigated even if this solution doesn't allow setting up a different level of biasing.

- Second Conversion.
  With gained experience in the 22GHz second conversion design we have reached a good integration level of this circuitry (two double channels and monitor TotalPower) . The carrier board , where the 2nd conversion is mounted, realizes a general purpose to supply, monitor and switch on/switch off several parts of RF devices. Future upgrade in 2nd conversion board could implement two more RF channels (polarisations) and the fixed synthesiser to be used as 2nd LO.
  The aluminium box where 2nd conversion board is inserted guaranties the necessary isolation to induced RF interferences from carrier board electronic devices.

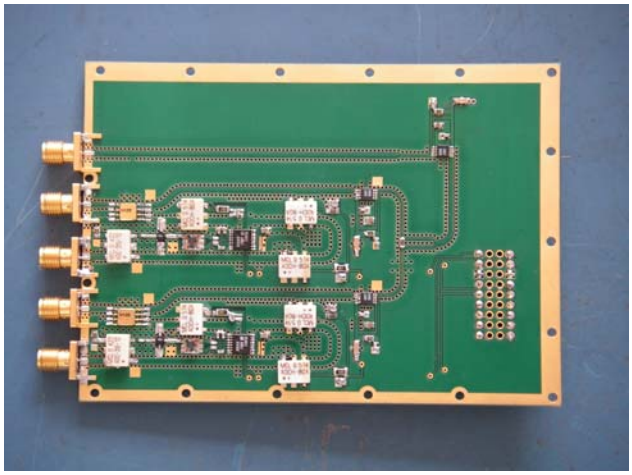

6.2 The injection of a noise calibrated signal into a huge amount of channels

- Injection of noise calibrated signal.
  For huge amount of feeds the signal could be injected by radio transmitted noise calibrated signal from primary focus. This solution needs to accurately evaluate the path attenuation (depending on the weather conditions).
  The classical solution in to inject the noise calibrated signal through a directional coupler. Since the expensive cost of Noise Generators are mainly due to their calibration rather than their technologies, we'll try to integrate into FEM a cheap noise source and then we'll accurately calibrate all, once the receiver will be working.
  The last solution suggested is to integrate the noise generator inside the LNA switching it on and off with a TTL command.

All the consideration above are necessary for dual conversion super-heterodyne architecture. If the goal of the receiver is to have high sensitivity total power instrument, the receiver (or better radiometer) must have an "ad-hoc" architecture as mentioned in chapters 3 and 7.
Both solutions could survive if a power splitter is inserted after the first LNA in order to parallelize the two architectures.

7. MATTERS ARISING FROM VERY LARGE BANDWIDTH SYSTEMS

A key subject arising from receiving systems using very large bandwidth is how much the classical radiometer formula is valid, or how much the system is dominated from white noise. It is known that effects other than white noise affect the minimum power detectable value (sensitivity): when this effects come into play is firstly depending on how much the receiving system is pushed at the extreme in terms of bandwidth. In fact the problem is not particularly felt in spectroscopy where the bandwidth is subdivided in smaller ones or in polarimetry where the problem is overcome by using correlator techniques. For both these reasons also VLBI doesn't suffer from this limitation. Very different is the situation when total receivers are used for observations of faint targets.
In the following a discussion will try to overview this subject both in general terms and in application at specific receivers.

7.1. Sensitivity depends on more than white noise

Firstly sketch the essential parts of a total power receiving system, fig.7.1.1

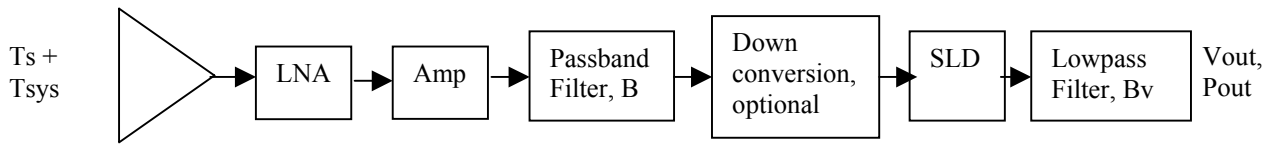

Fig. 7.1.1

At the input of the horn there is the contribution of the target we want to measure and the overall noise of the receiving system; this last is the sum of receiver noise plus many other additional contribution coming from sky, atmosphere and antenna optics (spillover).

$$Ts = Tsource \tag{7.1.1}$$
$$Tsys = Tric + To \tag{7.1.2}$$

The receiving system is composed by an LNA (Low Noise Amplifier), usually cooled at cryogenic temperature, a cascade of post-amplifiers (here concentrated in only one), a passband filter shaping the RF (radiofrequency) band large B. Then, if needed, there is a down conversion stage and finally a Square Law Detector with its lowpass filter defining the so called Video Bandwidth, Bv wide.
The video bandwidth sets also the integration time t of the total power; the relationship between t and Bv is[1]

$$t = \frac{1}{2 * Bv} \tag{7.1.3}$$

The powers at the input of the horn and at the output of the receiver are,

$$Pin = k * (Ts + Tsys) * B \tag{7.1.4}$$
$$Pout = k * (Ts + Tsys) * B * G \tag{7.1.5}$$

where G is the overall power gain of the receiver, including the responsivity of the SLD diode.
What we want to measure is Ts and its variation. To be sensitive at an amount equal to ΔT as low as possible the way is increasing the integration time given by the following

[1] For the purpose of this feasibility study is enough to consider an ideal integrator.

$$\frac{\Delta T}{Tsys} = \frac{1}{\sqrt{B * t}} \tag{7.1.6}$$

But, in principle, if Pout is increased/decreased of a ΔT amount it could be due not only from Ts input variation but also from G and Tsys variation. In fact we could write the same Pout + ΔPout as

$$Pout + \Delta Pout = k * (Ts + Tsys + \Delta T) * B * G \qquad \text{or} \tag{7.1.7}$$

$$Pout + \Delta Pout = k * (Ts + Tsys) * B * (G + \Delta G) \tag{7.1.8}$$

From the same two formulas we could calculate the amount of ΔT due to a ΔG (better, ΔG/G) variation, in fact equating (7.1.7) and (7.1.8) and using (7.1.5) we find

$$\frac{\Delta T}{Tsys} = \frac{\Delta G}{G} \tag{7.1.9}$$

In a similar way, using (7.1.7) and

$$Pout + \Delta Pout = k * (Ts + Tsys + \Delta Tsys) * B * G \tag{7.1.10}$$

we find ΔT = ΔTsys i.e.

$$\frac{\Delta T}{Tsys} = \frac{\Delta Tsys}{Tsys} \tag{7.1.11}$$

(7.1.6), (7.1.9) and (7.1.11) are three different statistical noise processes each variance of which being $(\Delta T)^2$. Because they are uncorrelated each other we can sum the variances in order to obtain the variance of the composed process, i.e. we obtain the well known formula

$$\frac{\Delta T}{Tsys} = \sqrt{\frac{1}{B * t} + \left(\frac{\Delta G}{G}\right)^2 + \left(\frac{\Delta Tsys}{Tsys}\right)^2} \tag{7.1.12}$$

The noise fluctuations of Tsys are mostly due to atmospheric fluctuations and they are overcome by using modulation techniques like *position switching* (by moving the antenna), *beam switching* (by using a second horn looking at the cool sky), *wobbling* (tilting, fastly enough, the secondary mirror of the antenna) and scanning on the source (on-the-fly mapping).

The noise fluctuations due to the variation of the overall receiver gain are more intriguing because they involve the technology of the active devices, their amount in the receiver chain and which ones are placed at cryo temperature and which ones are not.
Looking at the literature about this subject (see [1], [2], [3], [4], [5]) we could summarize these sentences:

a) The noise spectral density $(\Delta G/G)^2$ is proportional to the number N of the amplification stages of the amplifier
b) A GaAs amplifier shows a factor of about 3 less noise spectral density of an InP amplifier
c) A cooled amplifier shows greater noise spectral density as its physical temperature is lower. For example, an InP-HEMT LNA has a factor of 6 increase from 300K to 20K.

d) The gain fluctuations originate from the fluctuation of the transconductance of the transistor, i.e. from $(\Delta Gm/Gm)^2$
e) The transconductance fluctuations are inversely proportional to the gate area and drain-source current density,

$$\left(\frac{\Delta Gm}{Gm}\right)^2 \propto \frac{1}{L * w * J} \tag{7.1.13}$$

where L, w and J are respectively length and width of the gate and current density. By deeply investigation, it has been found that the HEMT transconductance should be stabilized as better as possible. The big cause for that is due to the stability of Drain current. The closed loop, servo Supply (*AliSrt*) is strongly suggested and it may reduce 1/f contribution up to 30%. Also LNA physical temperature should be stabilized as better as possible.

f) Measurements on InP-HEMT amplifier at 3.8mm show a spectral noise density following this law,

$$\left(\frac{\Delta G}{G}\right)^2 = N * A * \left(\frac{1}{f}\right)^{\alpha} \tag{7.1.14}$$

with A= $3.6*10^{-8}$ Hz^{-1} per stage and N= number of stages. A is also stated as the value of the noise spectral density in a bandwidth wide 1Hz. The term α is chosen 0.9-1 in the simulations but direct measurements ([2], [3]) show a value down to 0.45!
The noise landscape can be depicted such that Fig. 7.1.2 where the $(1/f)^{\alpha}$ trend (pink squared) is intercepted by the white noise horizontal lines (red lines). Each line defines a different value of white spectral density. In this case where the bandwidth is fixed, this means the white spectral density is defined by the integration times t. It is worth noting that any horizontal line intersect the 1/f trend at different frequency values, each of them is the value where 1/f noise and white noise are equal.

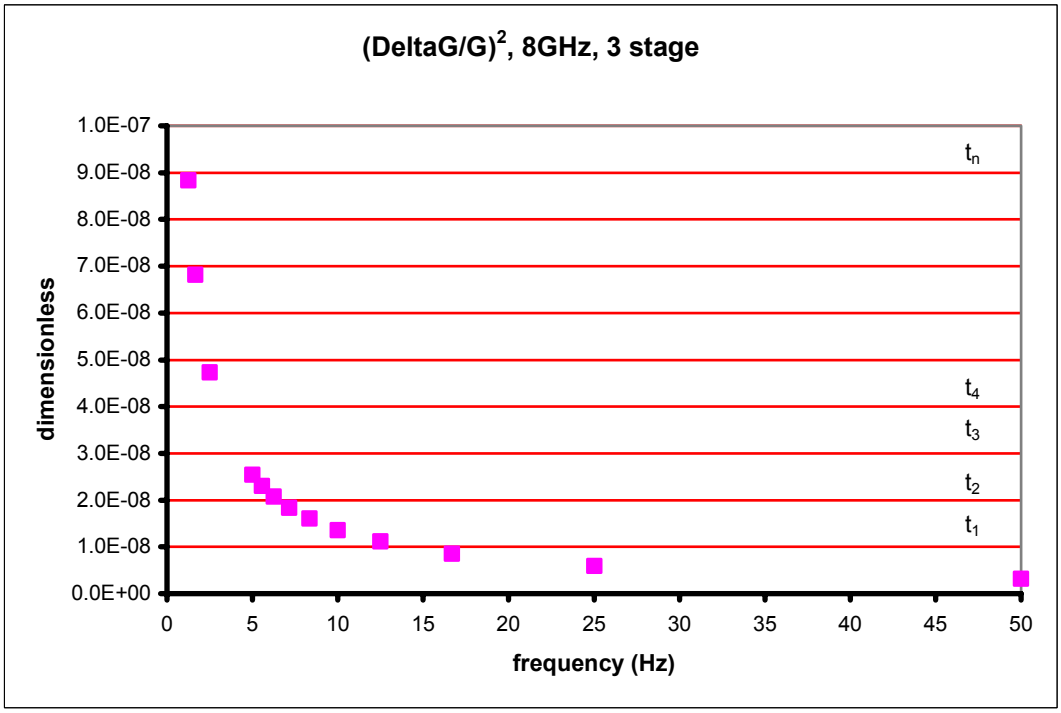

Fig. 7.1.2

g) Reference [6] shows that an accumulation of many samples of integration times (7.1.3), in presence of 1/f noise, increase the noise contribution. In general

$$\int_{1/T}^{Bv} \left(\frac{\Delta G}{G}\right)^2 df = \frac{N*A}{1-\alpha} * \left(B_v^{\,1-\alpha} - \frac{1}{T}^{1-\alpha}\right) \qquad (7.1.15)$$

where T is the total integration time; it must be B_v>>1/T, or T>>t.
In a simplified case α=1, $(\Delta G/G)^2 * B_v$ becomes N*A while (7.1.15) becomes

$$N*A*\ln(B_v*T) \qquad (7.1.16)$$

with B_v*T>>1. Therefore the extra noise factor due to long integrations is ln(Bv*T).

It can be useful adding here some graphs showing how the situation changes by switching from usual bandwidths to large and very large ones.
In VLBI RF band on the order of 10MHz are usual, total power observations can range up to B=100MHz, while the value we consider for large and very large bandwidth is B=2 and 8GHz. In the following four graphs, Fig. 7.1.3 to 7.1.6, values comparing (7.1.6) and (7.1.12), neglecting the fluctuations of Tsys, are shown for these four different values of B, i.e different bandpass filtering in fig. 7.1.1.
They are plotted against integration time coming from different lowpass filter values of fig.7.1.1.
The LNA is thought to be a three stage InP device, α is chosen to be 0.9.
Like expected, as B is increased the positive effect of bandwidth is lost because the amount of $(\Delta G/G)^2$ become equal and greater than of (1/Bt) and this happens to begin from lower and lower values of integration time as B increases: taking an excess noise (i.e the dT/Tsys divided for √1/Bt) of about 1.1 we have
t=0.3s for B=0.01GHz and dT/Tsys=$6.34*10^{-4}$;
t=0.09s for B=0.1GHz and dT/Tsys=$3.66*10^{-4}$;
t=0.02s for B=2GHz and dT/Tsys=$1.76*10^{-4}$;
t=0.009s for B=8GHz and dT/Tsys=$1.30*10^{-4}$

For example, comparing B=0.1GHz with B=8GHz we have a factor of 80 in bandwidth increasing in order to obtain only a factor of 2.8 in sensitivity! For t=0.09s we instead would dT/Tsys=$0.4*10^{-4}$ with B=8GHz, a factor of √80, like in white noise dominated total power systems.

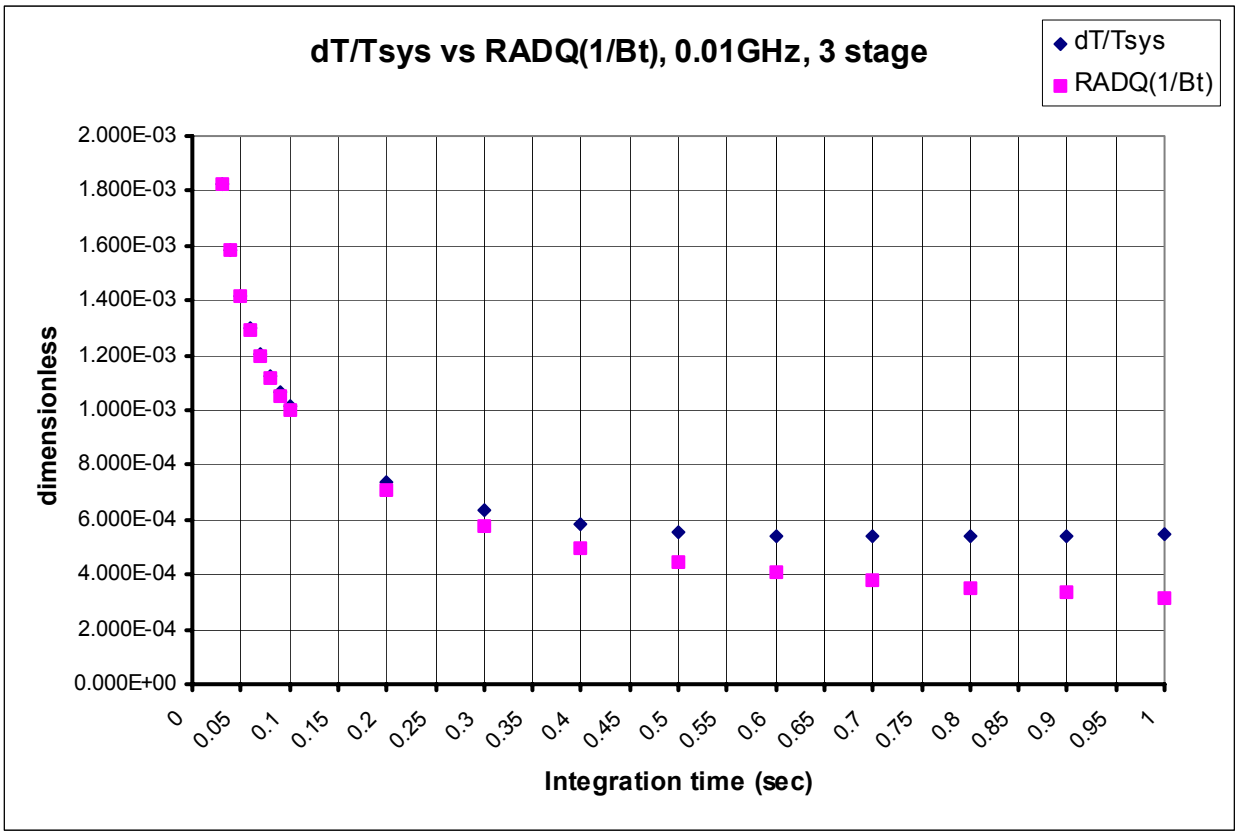

Fig. 7.1.3

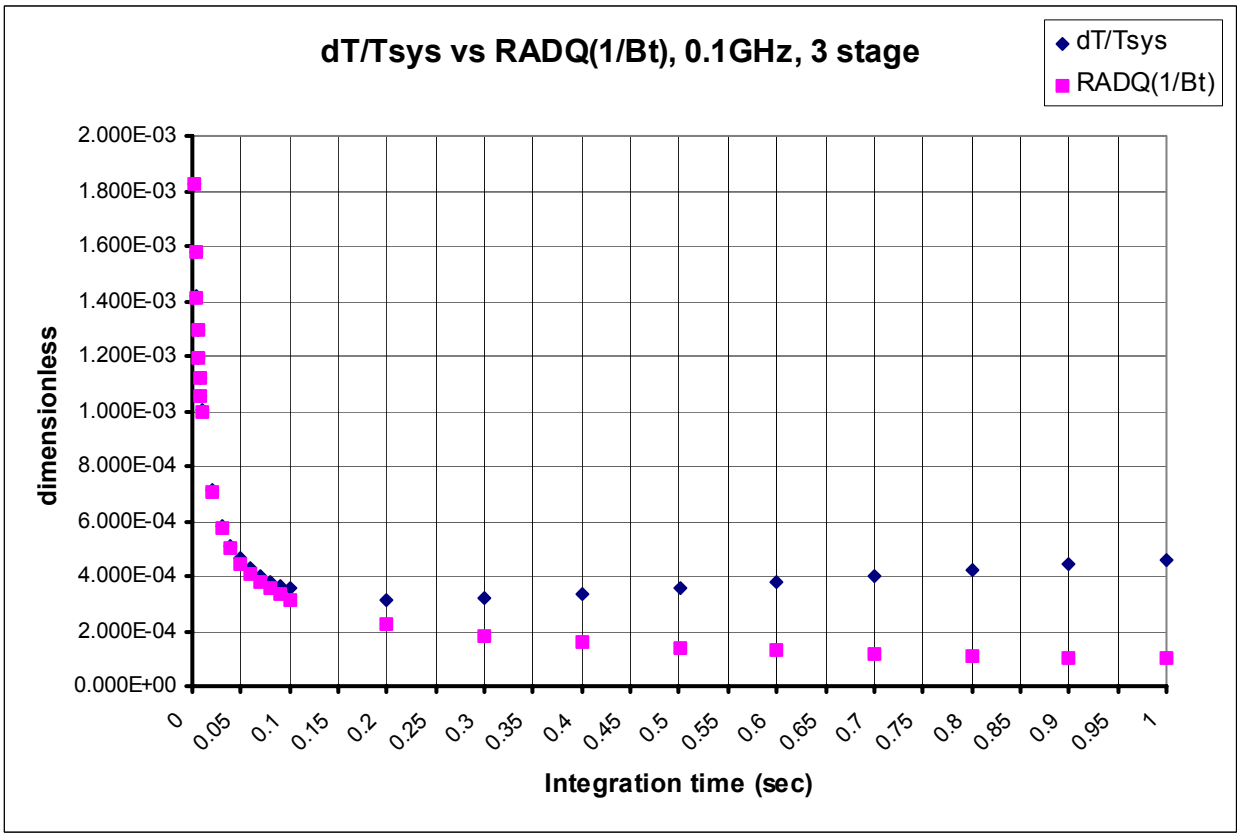

Fig. 7.1.4

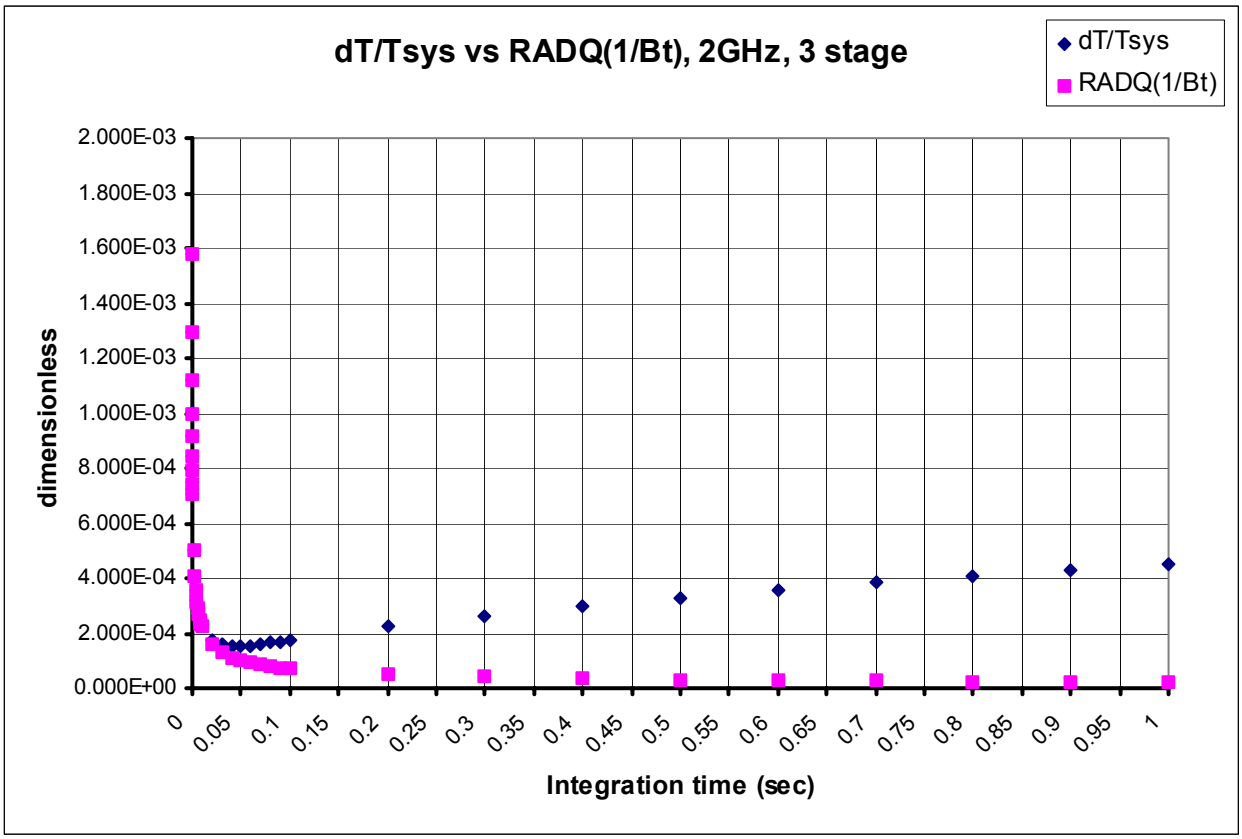

Fig. 7.1.5

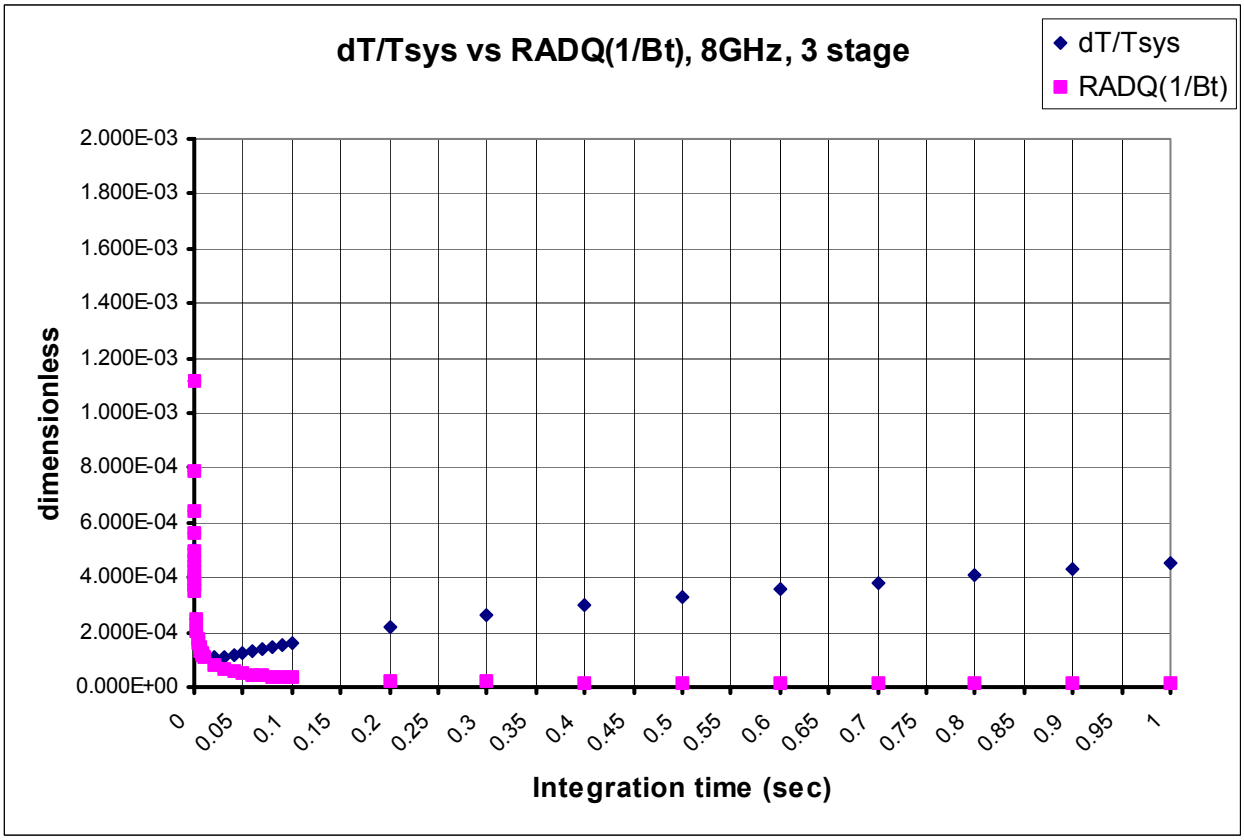

Fig. 7.1.6

A different way to explain the 1/f matters is to put into relation the Allan Variance versus the integration time [7]. The latter shows immediately the maximum integration time by looking at the slope of the curve (slope=-1 is for white noise, slope=0 is 1/f contribution and slope>0 is for worst drift contributions).
With this type of representation, one can easily identify the type of the noise present, and determine what is the optimum integration time to get the best sensitivity. This time limit is called Allan Time, integrating more than this would not give any improvement and could even degrade the signal to noise ratio.

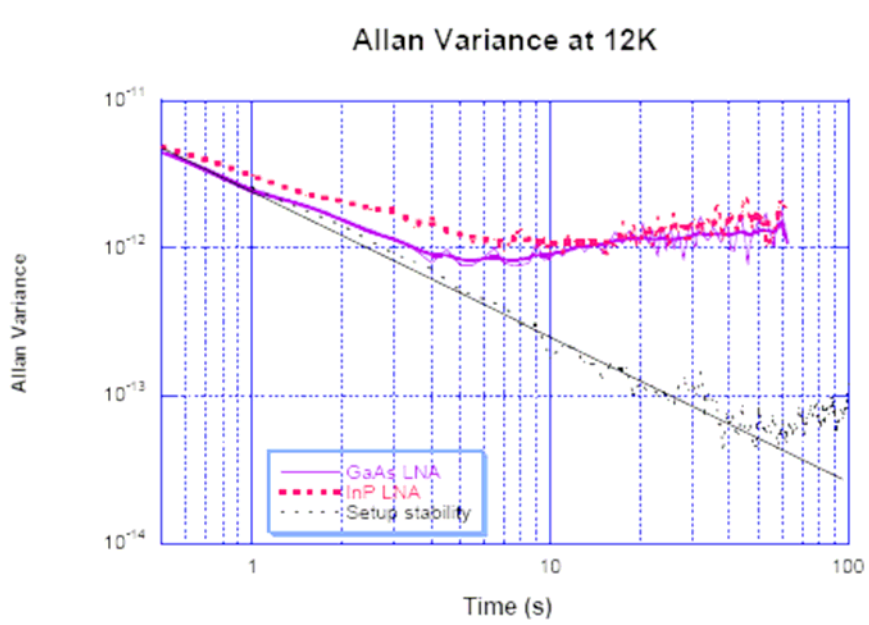

Fig. 7.1.7

7.2. Which components are responsible of 1/f noise value in a receiver chain

In the previous paragraph we have reported the 1/f noise values for a single 3-stage LNA, but looking at Fig. 7.1.1 the receiver chain is composed of many active devices. We here refer to "active devices" to those ones made by semiconductors, in which a physical 1/f phenomena arises. Thus we refer to amplifiers and the SLD diode, G_{lna} is the cryo amplifier gain, G_a is the total gain of the warm post-amplifiers, R is the responsivity of the diode and G_v is the total gain in the post detection stage.
The active gain, without considering the attenuation throughout the receiver chain, can be written:

$$G = G_{\ln a} * G_a * R * G_v \qquad \text{and} \tag{7.2.1}$$

$$dG = \left(\frac{\partial G}{\partial G_{\ln a}}\right) dG_{\ln a} + \left(\frac{\partial G}{\partial G_a}\right) dG_a + \left(\frac{\partial G}{\partial R}\right) dR + \left(\frac{\partial G}{\partial G_v}\right) dG_v \qquad \text{thus} \tag{7.2.2}$$

$$\frac{\Delta G}{G} = \frac{\Delta G_{\ln a}}{G_{\ln a}} + \frac{\Delta G_a}{G_a} + \frac{\Delta R}{R} + \frac{\Delta G_v}{G_v} \tag{7.2.3}$$

If we look at $(\Delta G/G)^2$ instead of $\Delta G/G$ we can consider the sum of the square of each term because the fluctuations of the devices are uncorrelated so the cross products are zero [1],

$$\left(\frac{\Delta G}{G}\right)^2 = \left(\frac{\Delta G_{\ln a}}{G_{\ln a}}\right)^2 + \left(\frac{\Delta G_a}{G_a}\right)^2 + \left(\frac{\Delta R}{R}\right)^2 + \left(\frac{\Delta G_v}{G_v}\right)^2 \tag{7.2.4}$$

Now, using the sentences reported in the previous paragraph we could say

A) LNA is an InP-HEMT amplifier and cooled, so its spectral density is 18 times that one of the warm post-amplifiers G_a (sentences a and b), supposing them GaAs devices. We should correct this factor for the amount of stages in the GaAs devices but two cases are readily shown:

a) direct detection receiver, no conversion. The block diagram after the cooled LNA may be like Fig.7.2.1

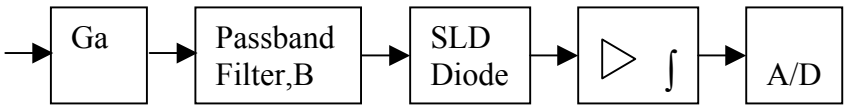

Fig. 7.2.1

considering 30dB of gain for the 3-stage LNA the pre-detection gain G_a is around 40dB[2], achievable with 4 stages, so the factor 18 reduce to about 13, mainteining negligible the G_a fluctuations.

b) superheterodyne receiver, tipically two conversions for large RF bandwidth.
The block diagram after the cooled LNA may be like Fig.7.2.2.
This case is more complicated due to the presence of many devices, but an active gain G_a around 50dB may be quoted, reducing the factor at 10 or slightly less.

B) G_v is the gain after the SLD and it is usually obtained by using low noise op-amp or instrumentation amplifiers. They show input voltage noise as low as some tens of nV/√Hz in the 1Hz bandwidth. Compared to the noise voltage due to the ΔG of the LNA, in 1Hz calculated at the same input, this means a value of the noise power many order of magnitude lower.

C) Similar considerations may be done for the detector diode: with the needed G, and a high responsivity (generally these zero bias diodes show 0.5-1V/mW@ 1MΩ load) the comparison between the LNA noise and the detector noise at the output of the SLD make this last negligible. Moreover we will use "zero bias" diodes which show nominally a zero 1/f noise contribution.

Finally we can answer the question placed at the beginning of the paragraph: in a receiver for radioastronomy, where we have high gain and cooled amplifier, the dominant element regarding the 1/f noise is the cryogenic low noise amplifier.

Anyway, in general and other than 1/f noise, many other contributions have to be careful controlled in the receiver. More causes of gain fluctuations could be

- Gain fluctuations due to RF gain temperature variations
- Gain fluctuations due to RF gain power supply instabilities
- Gain fluctuations due to conversion factor diode for temperature variations
- Gain fluctuations due to conversion factor diode for power supply instabilities
- Gain fluctuations due to LowFrequency gain temperature variations
- Gain fluctuations due to LowFrequency gain power supply instabilities
- Gain fluctuations due to mechanical stresses of cables

[2] Referring Fig.1.1 and considering RF=22GHz, B=8GHz, Tsys=60K, P at the input of SLD= -20dBm, we have Pin≈ -82dBm, therefore Glna + Ga= 62dB and Ga=32dB. We need a little more than this because of filters, circulators and pads inserted in the chain.

Some empirical data could be added in order to get an order of magnitude,
a) LNA: due to Id variations,

For LNAs self-biased forming a thermally compensated DC network, so NOT biased with a Servo Power Supply (i.e. AliSRT board developed in the Faraday subproject2), the expected behaviour of the Id vs. temperature may be roughly estimated in ≈ 30 µA/°C.
Given some experimented behaviour of Gain vs Id, of ≈ 0.006 to 0.020 dB/mA for every dB of Gain, for the following typical case:
LNA: Gain ≈ 30 dB
Cryostat: Observed temperature changes +/- 0.7 K /day (say 32µK/sec)

We'll get the following rough estimation of long term variations:
$\Delta G^{dB} \approx 0.2$ to 0.6 dB/mA
$\Delta G^{dB} \approx$ 6mdB/K to 20mdB/K
$\Delta G^{dB} \approx 0.2$ µdB/sec to 0.6 µdB/sec .

Note that, usually, temperature variations inside a dewar refrigerated by a close cycle He, will change more quickly and synchronously with 1 Hz pumping sound. So for timescales of exactly 1 sec. the variations may be higher.

b) Coax Cables: due to temperature

Given the experimented behaviour of coax cables vs temperature, of ≈0.0013 dB/(dB °C), a variation of 10°C during 8h long day will give a rough estimation of $\Delta G^{dB} \approx 0.4$ µdB/sec every dB of cable attenuation, i.e. for a 10 dB loss coax cable, $\Delta G^{dB} \approx 4$ µdB/sec

c) Coax Cables: due the movement, flexion, and small non-destructive torsion.

Given the experimented behaviour of coax cables vs flexure, of ≈0.03 to 0.3 dB/(¼ turn), a smooth tracking movement of 180° over 8 h will give a rough estimation of $\Delta G^{dB} \approx 1$ to 10 µdB/sec for every flexions.

These ΔG data are given in term of dB, it holds the following,

$$\frac{\Delta G}{G} = 10^{\frac{\Delta G(dB)}{10}} - 1 \qquad (7.2.5)$$

Typical values are then summarized in the following table,

$\frac{\Delta G}{G}$	ΔG^{dB}
1E-7	0.43 µdB
1E-6	4.3 µdB
1E-5	43 µdB
1E-4	0.00043 dB

Tab. 7.2.1 G fluctuations in linear and dB units

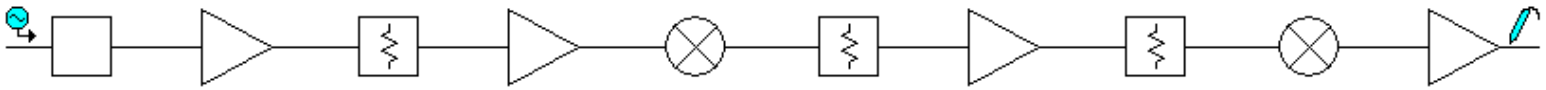

	LNA	Cavi Dewar	Post LNA	MZ5010C	Circolatore	JCA48-100	Filtro, coax	M93C	ERA2+6	Cascade Total
NF (dB)	0.02	0.28	1.2	1.5	9.5	0.2	2.2	1	8	4.5	2.78
Gain (dB)	-0.1	26	-1.2	16	-9.5	-0.2	12	-1	-8	23	57.00
OIP3 (dBm)	100	15	100	14	6	100	20	100	8	33	24.80
Pout (dBm)	-81.1	-55.1	-56.3	-40.3	-49.8	-50.0	-38.0	-39.0	-47.0	-24.0	
NF+ (dB)		0.16	0.00	0.00	0.00	0.00	0.00	0.00	0.00	0.00	
OIP3+ (dB)	0.00	0.03	0.00	1.44	0.97	0.00	0.56	0.00	1.19		

Input Power (dBm)	-88.00			Input IM (dBc)	
S/N (dB, Required)		S/N (dB, Actual)	7.83	Input IP3 (dBm)	-32.20
		Sensitivity (dBm)	-88.83	Output IM Level (dBm)	-121.60
Losses (dB)	0	MDS (dBm)	-88.83	Output IM Level (dBc)	-97.60
System BW (MHz)	2000	Noise Temp (K)	22.41	SFDR (dB)	37.75
Source Temp (K)	25				

Fig. 7.2.2

NOTE: the measured cooled LNA gain is 30dB. The value reported in the simulation is for warm amplifier.

7.3. Modulation techniques for overcoming 1/f noise

Before to start with a survey of techniques able to overcome gain fluctuation effect we must introduce the knee frequency parameter.
Looking at (7.1.6) and (7.1.9) we have seen two noise spectral densities. The latter has been defined as (7.1.14), showing a decreasing as the frequency increases, the former is constant. A rough time scale of the gain fluctuations is defined as *knee frequency*, the frequency at which the total noise spectral density of the 1/f effect take the same value of the white noise effect. This means we have to equate (7.1.14) and (7.1.6). So we have

$$\frac{1}{B*t} = N*A*\left(\frac{1}{f_{knee}}\right)^{\alpha} \qquad \text{from which we have} \tag{7.3.1}$$

$$f_{knee} = \left(N*A*B*t\right)^{\frac{1}{\alpha}} \tag{7.3.2}$$

Showing that the knee frequency value is not an invariant for the receiver or LNA, in fact it increases as the constant noise floor due to white noise is lowered by increasing B or t.
The several available modulation techniques all rely on the detection of the difference between the input of the receiver and a known, and stable, noise source [8,9,10,11,12,13]. In term of frequency domain this means to shift the output of the SLD from baseband (from DC to the value of Bv) to values around a known frequency, called *chopping frequency*. The bandwidth around f_{chop} is Bv.
In this way the low frequency components of the output noise spectrum, including those ones less than f_{knee}, are skipped and the value of $(\Delta G/G)^2$ at f_{chop} is negligible .
At the end of this chapter a brief review of different radiometer architectures are reported. They show pros and cons but principally add a lot of components in view of a multifeed realization.

In order to recover the signal present at the receiver input the output of the SLD is demodulated by using a synchronous modulator before the integrator. The receiver of Fig. 7.1.1 becomes

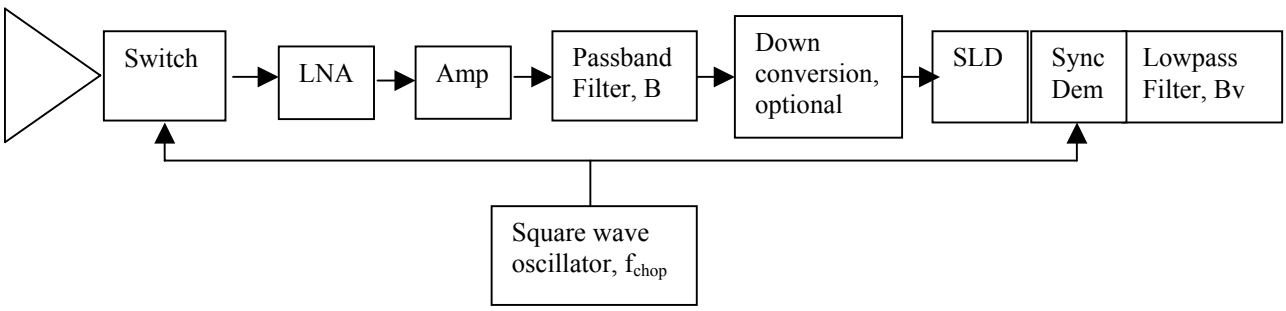

Fig. 7.3.1

These schemes mostly provide lossy components, the switch before the LNA, so increasing the receiver noise. Further the Dicke scheme they provide an AGC for changing the value of the noise source in order to follow the variable value of the input receiver noise. In fact the known formula of the Dicke radiometer [13]

$$\frac{\Delta T}{Tsys} = \frac{\Delta G}{G} * \frac{To - Tref}{Tsys} \tag{7.3.3}$$

should fail because To**,** comprising the atmopshere contribution, varies a lot with elevation (especially at frequencies higher than 20GHz) so the nulling effect of the reference load Tref doesn't work. Moreover even if atmosphere shouldn't be a problem radioastronomy will to observe sources giving very different antenna temperature, while Tref is fixed. Instead, if the switch is replaced with a directional coupler and a known and stable noise source (both these components are usual in radioastronomy receivers) is switched on and off at the frequency f_{chop}, for half period the receiver sees Ts+Tsys, for the following half period it sees Ts+Tsys+Tref so we have,

$$\mathrm{Pout_1} = k * (\mathrm{Ts} + \mathrm{Tsys}) * B * G \tag{7.3.4}$$

$$\mathrm{Pout_2} = k * (\mathrm{Ts} + \mathrm{Tsys} + \mathrm{Tref}) * B * G \tag{7.3.5}$$

The synchronous detector detects the difference between these two values so at the output of the integrator we have

$$\mathrm{Pout_2} - \mathrm{Pout_1} = \Delta\mathrm{Pout} = k * (\mathrm{Tref}) * B * G \tag{7.3.6}$$

In this scheme we could write the same ΔPout as

$$\Delta\mathrm{Pout} = k * (\mathrm{Tref} + \Delta T) * B * G \qquad \text{or} \tag{7.3.7}$$

$$\Delta\mathrm{Pout} = k * (\mathrm{Tref}) * B * (G + \Delta G) \tag{7.3.8}$$

(7.3.7) highlights that a variation ΔT occured with respect to the stationary value (7.3.6); instead (7.3.8) gives the source of variation to a G changing equal to ΔG; equating (7.3.7) and (7.3.8)

$$\frac{\Delta T}{\mathrm{Tsys}} = \frac{\Delta G}{G} * \frac{\mathrm{Tref}}{\mathrm{Tsys}} \tag{7.3.9}$$

Comparing (7.3.9) with (7.1.9) we see the fluctuations could be attenuated by a factor Tref/Tsys.
If the noise cal reference is on the order of one tenth of Tsys or less the spectral noise density of gain fluctuations is attenuated by a factor of 100. At the highest frequencies, greater than 20GHz where so large bandwidth can be used, the Tsys values increase more and more (let's say from 40 to 250K, depending both on frequency and antenna elevation), therefore, because it is not difficult to provide Tref on the order of some kelvin, the ratio Tref/Tsys can be very low. It is worth noting that the positive function of Tref is valid at each elevation, because the damping effect relies on a ratio and not on a difference like in (7.3.3).
Using (7.1.14) it is like that the A value should be now 100 times lower and, very important, the frequency value to which ΔG/G is effecting is now f_{chop} and not Bv! In this case Fig. 7.1.3 to 7.1.6 do not represent anymore the behaviour of the system, i.e.

a) the value of fluctuation is

$$\left(\frac{\Delta G}{G}\right)^2 = N * A * \left(\frac{\mathrm{Tref}}{\mathrm{Tsys}}\right)^2 * \left(\frac{1}{f_{chop}}\right)^{\alpha} \tag{7.3.10}$$

Now, in the chopped total power radiometer, we are free to fix the amount of excess noise due to gain fluctuation with respect the white noise value (ideally 0%).

The chopping frequency is chosen such that the excess of noise due to gain fluctuations is less than 1+ε times the white noise, i.e. must be verified

$$\frac{\sqrt{\frac{1}{B*t}+N*A\left(\frac{1}{f_{chop}}\right)^{\alpha}}}{\sqrt{\frac{1}{B*t}}}\leq 1+\varepsilon \qquad (7.3.11)$$

and by using (7.3.2)

$$f_{chop}\geq\frac{f_{knee}}{[\varepsilon*(\varepsilon+2)]^{1/\alpha}} \qquad (7.3.12)$$

b) due to the very low value of the fluctuation noise, the system is dominated by the white noise only so

c) we can choose the integration time as large as necessary, because now in practice it doesn't affect the ΔG/G value.

Anyway in a chopped total power radiometer also the white noise formula with respect to an ideal total power is affected. This is because the chopping and its inherent differential working principle makes useful only half of the integration time, which one where the noise cal is off and, in addition, the average noise temperature is higher than Tsys.
It could be shown that (see Appendix to this chapter)

$$\Delta T=\sqrt{2}*\frac{Tsys}{\sqrt{B*t}}*\sqrt{1+\frac{1}{x}+\frac{1}{x^2}} \qquad (7.3.13)$$

where x = Tref/Tsys.
The factor √2 comes from the statistics of the difference between the power with and without the reference injection. The factor containing the x parameter comes from the fact that in order to correct for the gain fluctuations the observable is

$$\frac{Pout_1}{Pout_2-Pout_1} \qquad (7.3.14)$$

so the propagation of errors on Pout_1 and Pout_2 by means of (7.3.14) determines the effect of x.
In order to avoid excessive degradation of ΔT with respect to ideal radiometer formula (7.1.6) a compromise about the x value will be mandatory. For practical reasons the level of Tref should be usually on the order of 0.1*Tsys or something like that. In this case, x=0.1, the factor under square root is 111 so the white noise should increase of more a factor of ten. On the other hand, looking at (7.3.13) Tref could be increased over x=1 paying only a factor of √3 or less in sensitivity degradation. Within this x range an optimum value have to chosen. Note that a high value of Tref could imply a corresponding high amount of ΔTref expressed in kelvin, such that to be higher of ΔT coming from (7.3.13): a good environment temperature stabilization of the noise diode is therefore important.

As a concluding remark we point out that the practical realization of a modulation system needs both of the (7.3.4) and (7.3.6) values so we cannot use a synchronous detector, because it gives the (7.3.6) value only. The differential detection will be done by off line data processing, provided that the speed of the data acquisition system is high enough to sustain the data rate and a sufficient precise time mark or, equivalently a flag on the data, is available in order to recognize the on-off transition times. A worth example of this off-line synchronous detection is the OBS+Toolbox data and processing acquisition system used at Effelsberg 100m telescope. Useful references where the chopping of a calibrated, and stable, noise source is used in order to measure the gain fluctuations are [14,15].

As an example, at Effelsberg the time t =16msec and the complete cycle time T = 32msec. The noise cal is thus chopped at 31.25Hz.
If we have antenna position switching or cross-scan or subreflector wobbling instead of beam switching (see next paragraph for definitions) the On and Off source switching is not immediate but we should take into account a longer cycle affecting the effectiveness of the atmosphere fluctuations recovering. Continuing to switch the cal diode during the antenna slew the receiver gain fluctuations could be traced also in this cases.

RADIOMETER DESIGNS

In this paragraph we are not interested in the mathematical and technical details but we will give a general description pointing out the pros and cons obtained using these techniques [16].

Switched radiometers- Dicke receiver

The simplest way to implement a differential radiometer is to switch the input of a total power radiometer between two sources to be compared, and demodulate the output of the radiometer synchronously with the toggling of the input switch. The switching upconverts the input signal to higher frequencies, chosen to be above the amplifier's knee frequency. The subsequent demodulation recovers the input signal by downconverting it to DC, but rejects signals related to the lower frequency amplifier gain fluctuations. For this technique to be effective |tsrc – tref| « Tsys, the magnitude of the difference signal to be measured must be small with respect to the system temperature. Non-idealities are characterized by toffset, the offset temperature; they result in a signal at the output of the radiometer even when comparing sources at the same temperature, and also this must be small compared to Tsys. Such designs put great demands on the performance of the switch at the input of the radiometer. The switch must have very low, stable losses and operate over wide bandwidths, often requiring the switch to operate at cryogenic temperatures. Ferrite switches have bandwidth limitations and relatively high loss, both of which greatly diminish radiometer performance. PIN diode switches also suffer from high loss. Where feasible, mechanical switches are often the best choice.
Such a switching scheme was feasible in this case since the switching frequency needed to ameliorate the gain fluctuations in this radiometer was only several Hz. The original 10 Hz knee frequency of the amplifier system was reduced to below 1 mHz at the radiometer output by implementing the switching.
This allowed for integration times approaching one hour to be employed to achieve the required sensitivity.
The typical switching frequencies are in the range 10Hz up to 10KHz.

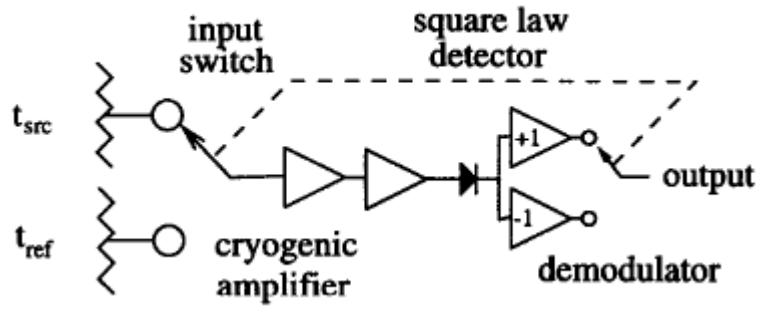

Correlation Radiometer

When the switching rate required to diminish the gain fluctuations exceeds several 10's of Hz., a correlation radiometer is often the best approach. In a simple correlation receiver the signals from the sources to be compared are connected to two ports of a hybrid tee, say the E and H ports. The output from the collinear ports are then separately amplified and fed into a mixer which acts as a correlator. Signals presented to the input of the radiometer are split between the two legs of the radiometer by the hybrid tee and hence have a fixed relative phase between the legs. The large noise signals due to the noise temperature of the amplifiers are uncorrelated (apart from crosstalk in the hybrid tee) since they arise from different amplifiers.

These uncorrelated signals, when applied to the two inputs of the mixer average to zero. However, the signals from the two sources, are correlated between the two legs of the radiometer and produce correlator outputs of opposite sign, since the signals originating from the E port of the hybrid are in phase when they reach the correlator and the signals from the source connected to the H-port are 180 deg out of phase at the correlator. In practice it is usually necessary to introduce another level of modulation by placing a 0/180 deg phase switch in one of the signal paths after the amplification. The output of the correlator is then demodulated synchronously with the toggling of the phase switch. This additional level of modulation is used to eliminate drifts due to nonidealities in the correlator. The hybrid combiner limits the maximum bandwidth of the radiometer, typically 10% of central frequency.

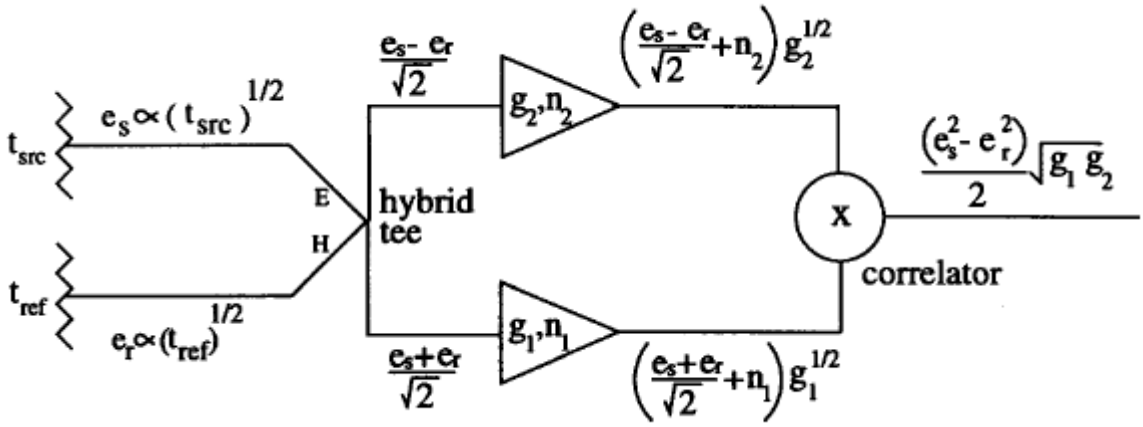

Hybrid Radiometer

Although correlation radiometers have excellent performance characteristics, they place very stringent requirements on the components of the radiometer.

Under these conditions a hybrid approach was deemed best. The hybrid design is similar to a true correlation radiometer, however after amplification the two signals are recombined in a second hybrid tee, the outputs of which are feed into two square law detectors, the outputs of which are then differenced. The large time spurious varying signals. due to the noise powers of each amplifier are divided equally between the detectors and therefore appear as a common mode signals which cancel when the detector outputs are differenced. Amplified signals from the two input sources appear at opposite detectors, so the difference of the detector outputs reflects the difference in the power emitted from the sources. This approach, augmented by phase switching to remove effects related to detector gain variations, lowered fknee of the outputs radiometers from 1 kHz to below 10 mHz (MAP W-band Radiometer).

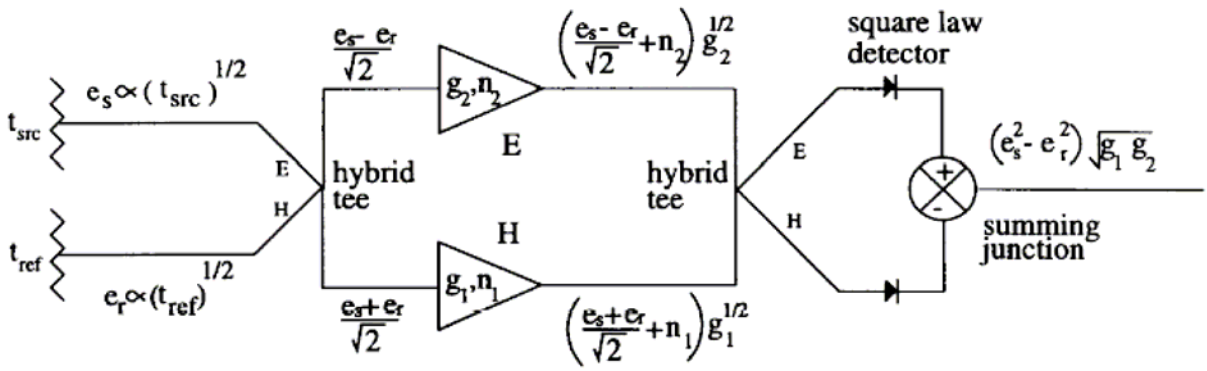

7.4. Modulation techniques for overcoming Tsys fluctuations

For Tsys fluctuations a similar landscape to which depicted for gain fluctuation arises. Here the modulation techniques are either mechanical (wobbling either the subreflector or the antenna) or electronic (using two receivers, one of them pointed ON the target and the other one OFF the target) or observative (*OTF mapping*). The mechanical and electronics methods are also known as *beam switching* techniques. The classical work reported in [17] is still valid, while [18] gives a comparison among these different techniques. As done before for gain fluctuations a cookbook can be summarized as the following:

a) The atmospheric fluctuations can be temporal variation (the brillance temperature of the atmosphere varies with time) or spatial variations (the brillance temperature of the atmosphere varies in space). Generally which one the two are to be considered depend on the extension of the source to be measured.
b) Common to all these techniques is that the blank sky should have the same amount of atmospheric contribution of the target line of sight, otherwise an offset at the output is seen due to non perfect cancelling during the differential on-off method. For this purpose the off acquisition should be at both opposite sides of the target.
c) In the mechanical chopping the frequency of the chop is mandatory; it should be faster than the atmospheric fluctuations. In principle the beam switching techniques work well if small angular beam throws and high switching frequencies are used. Optimum values of beam throw and switching frequency should however be based on a good characterization of the atmospheric fluctuations at the site. The first cause of variation inherent of this technique is a temporal variation. As the chopping frequency is increased the error due to atmospheric fluctuations decrease while the system noise per half cycle increase.
d) The OTF mapping seems the most promising strategy; again an high rate scanning of the antenna is important. The off positions are taken at the beginning and at the end of each stripe for each coordinate, slightly out the edges of the stripe. The first cause of variation inherent of this technique is a spatial variation, depending on as large as the source to be mapped.
e) The goal of each Tsys fluctuations removal is that its residual noise be less than the system noise. In this case the observation will not be limited by errors in atmospheric subtraction. If this shouldn't be the case double beam switching and OTF mapping are able to average down the residual atmospheric noise.

REFERENCES

1. E. J. Wollack
"High-electron-mobility-transistor gain stability and its design implications for wide band millimeter wave receivers" Rev. Sci. Instrum vol. 66, pag. 4305-4312 (August 1995)
2. E.J. Wollack, M.W. Pospieszalski
"Characteristics of broadband millimeter-wave amplifiers for radiometry"
IEEE MTT-S Digest, 1998, pag. 669-672
3. M.W. Pospieszalski, E.J. Wollack
"Characteristics of broadband InP HFET millimeter wave amplifiers and their applications in radioastronomy receivers" Proc. of ESA Workshop on mm-wave, Helsinki, May 1998
4. M.W. Pospieszalski, E.J. Wollack, J. Webber
"MMA Receivers: HFET amplifiers" MMA Project Book, Chapter 5, Section 4, 1999
[5] N.C. Jarosik, "Measurements Of The Low-Frequency-Gain Fluctuations Of a 30 GHz High-Electron-Mobility-Transistor Cryogenic Amplifier", 1996.
6. S. Weinreb "Radiometer sensitivity and transistor gain fluctuations"and its addendum, 1998 private communication to the authors of this report
7 C. Risacher, V. Belitsky
„GaAs-Based cryogenic amplifier for ALMA 2SB Mixer" ALMA Memo 421
8. M.E.Tiuri
"Radio Astronomy Receivers"
IEEE Transactions on Antennas and Propagation AP-12, 930 (1960)
9. J.V. Velley, B.F.C. Cooper
"An operational ruby maser for observations at 21cm with a 60-foot radio telescope"
Rev. Sci Instr. vol. 32, February 1961
10. J.P. Hach
"A very sensitive airborne microwave radiometer using two reference temperatures"
IEEE Transactions on Microwave Theory and Techniques, MTT-16, no.9, September 1968
11. G.D. Nicolson
"A gain stabilized maser radiometer for 13cm"
IEEE Transactions on Microwave Theory and Techniques, MTT-18, 169, 1970
12. M.J. Yerbury
"A gain stabilizing detector for use in radio astronomy"
Rev. Sci Instr. vol. 46, February 1975
13. K. Rohlf, T.L. Wilson
"Tools of Radioastronomy" 4th ed. Springer, pag.65
14. F. Ghigo
"K-band Continuum tests, February 15 2004" GBT note
15. C.J. Chandler, W.F. Brisken, B.J. Butler, R.H. Hayward, B.E. Willoughby
"Results of water vapour radiometry tests at the VLA" EVLA memo 73
16 N.C. Jarosik
"The use of Cryogenic amplifier in wide band radiometers", 2000.
17. Emerson D.T., Klein U., Haslam C.G.T.
"A multiple beam technique for overcoming atmospheric limitations to single-dish observations of extended radio sources" A&A 76, 92-105, 1979
18. Holdaway M.A., Owen F.N., Emerson D.T.
"Removal of atmospheric emission from total power continuum observations"
MMA Memo no. 137, September 1995

A7 - APPENDIX to chapter 7

In this appendix we outline a scheme of observation in order to use a total power radiometer with gain fluctuations corrected. In fig. A7.1 a scheme of a modulation radiometer is sketched

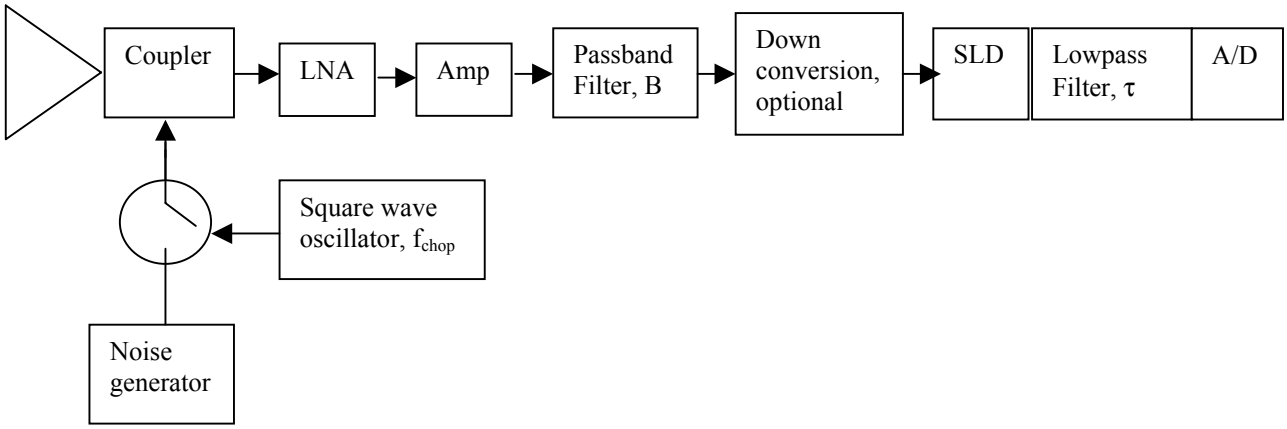

Fig. A7.1 Modulation receiver

1) The modulation period is T and, as said in 7.3 paragraph, it lies in the range 10÷100msec. This means that the hardware integration period t ranges 5÷50msec. This put the value of the ideal RC filter time constant τ (we choose 6*τ before sampling each data point, in order to get an accuracy of 0.25%)

$$\tau = \frac{t}{6} \tag{A7.1}$$

2) The situation at the output of the filter, in volt representing a power, or the A/D, in counts representing a voltage/power is depicted in fig. A7.2,

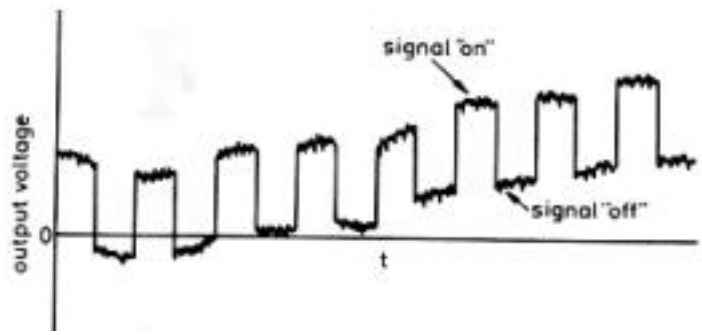

Fig. A7.2 Output of a modulated receiver

Each period is called cycle. Every period we get the observables,
Pi = power with cal off at the cycle i =kBGi(Tsys+Ts), Ts usually negligible
Pi^m = power with cal on at the cycle i =kBGi(Tsys+Ts+Tref)

3) Known (Pi, Pi^m) we will obtain the gain in the cycle i:

$$Gi = \frac{Pi^m - Pi}{kBT_{ref}} \tag{A7.2}$$

so we can get the power corrected for the gain,

$$\frac{Pi}{Gi} = kBT_{ref}\frac{Pi}{Pi^m - Pi} \qquad (A7.3)$$

In order to the system be working well must be

a) Gi constant within the cycle i
b) Tref and B constant anytime
c) Tsys constant within the cycle i

Hypotesis a) is necessary for (A7.3) be valid. Hypotesis b) is necessary for integrating many of Pi/Gi without having fluctuations. Hypotesis c) is necessary for (A7.2) be valid, only in this case the term kBGiTsys is equal in Pi and Pi^m. If this is not the case ,

$$Pi^m - Pi = kBGiT_{ref} + offset(i) \qquad (A7.4)$$

The offset should rise a new source of fluctuation on the observable.
Note that if the three hypotesis are valid the gain correction procedure by modulation works any thing is doing the antenna, on source, slewing, off source, etc. because the duration of each cycle is very shorter than the time scale of the antenna beam moving.
So all calculated points Pi/Gi are only affected by white noise: the calculation of the rms noise is the subject of this appendix and it can be regarded as inaccuracy of the value Pi/Gi or minimum detectable signal. In order to calculate such inaccuracy we need to use the *propagation errors formulae* applied to the (A7.3)[3].
We call

σi = inaccuracy of Pi
σi^m = inaccuracy of Pi^m

thus

$$\text{inaccuracy of } Pi^m - Pi = \sqrt{\sigma_i^2 + \sigma_i^{m\,2}} \qquad (A7.5a)$$

$$\text{inaccuracy of } \frac{Pi}{P_i^m - Pi} = \frac{Pi}{P_i^m - Pi} * \sqrt{\left(\frac{\sigma_i}{Pi}\right)^2 + \frac{\sigma_i^2 + \sigma_i^{m\,2}}{\left(P_i^m - Pi\right)^2}} \qquad (A7.5b)$$

Therefore using (A7.3) and re-arranging by noting that $Pi=kBG_iTsys$ and $Pi^m - Pi=kBG_iTref$ we have,

$$\text{inaccuracy of } \frac{Pi}{Gi} = \sqrt{2} * \frac{\sigma_i}{Gi} * \sqrt{1 + \frac{1}{x} + \frac{1}{x^2}} \qquad (A7.6)$$

where x = Tref/Tsys.
Note that if we divide each member of the (A7.6) for kB the meaning of "inaccuracy of Pi/Gi" and "σi/Gi", that are powers at the input of the receiver, change to "temperature inaccuracy of the i-point in a modulated total power system", i.e. ΔT, and the "temperature inaccuracy of the unmodulated acquired i-point", i.e. the white noise formula, so we can write, remembering that t=T/2

[3] $(A\pm\sigma_A) \pm (B\pm\sigma_B) = (A\pm B) \pm \sigma_{AB}$ with $\sigma_{AB}=(\sigma_A^2+\sigma_B^2)^{0.5}$;
$(A\pm\sigma_A)/(B\pm\sigma_B) = (A/B) \pm \sigma_{AB}$ with $\sigma_{AB}=(A/B)*((\sigma_A/A)^2+(\sigma_B/B)^2))^{0.5}$

$$\Delta T = \sqrt{2} * \frac{Tsys}{\sqrt{B * \frac{T}{2}}} * \sqrt{1 + \frac{1}{x} + \frac{1}{x^2}} \tag{A7.7}$$

This formula tells us how the sensitivity change in a modulated white noise dominated system. Note that in the meantime the receiver is modulated, the antenna goes on and off source and we'll integrate n CAL on source cycles and n CAL off source cycles so getting their difference in order to calculate the mean value of the temperature source and its deviation. That is we'll do

$$\mu_{on} = \left(\frac{1}{n} * \sum \frac{Pi}{Gi}\right)_{on} = \text{average value of n cycles on source} \tag{A7.8}$$

$$\mu_{off} = \left(\frac{1}{n} * \sum \frac{Pi}{Gi}\right)_{off} = \text{average value of n cycles off source} \tag{A7.9}$$

$$\frac{k * B * \Delta T}{\sqrt{n}} = \text{ inaccuracy of } \mu_{on} \text{ and } \mu_{off}\text{, supposed the same}$$

Because of we'll do

$$Ts = \frac{\mu_{on} - \mu_{off}}{k * B} \tag{A7.10}$$

the inaccuracy of Ts will be

$$\Delta Ts = \sqrt{2} * \frac{k * B * \Delta T}{k * B * \sqrt{n}} \tag{A7.11}$$

thus

$$\Delta Ts = 2 * \frac{Tsys}{\sqrt{B * n * \frac{T}{2}}} * \sqrt{1 + \frac{1}{x} + \frac{1}{x^2}} \tag{A7.12}$$

The amount of n depends on the time scale of the Tsys fluctuations. The switching on and off source, by the antenna or whatever else, must be faster than that time scale, exactly the same situation met for the receiver gain fluctuations.

8. SENDING A LOT OF LARGE BANDWIDTH CHANNELS TO THE BACK-ENDs

In view of realizing a new generation of receivers with a lot of beams a direct consequence is the availability of tens of channels to be processed by back-ends. Therefore the matter is how to deliver this huge amount of large bandwidth signals at the input of the continuum, spectroscopic and VLBI processors. In the following starting considerations from a system design point of view are sketched.

8.1 Overview of the data rates

In the previous chapters we summarized that the bandwidths we could have to face span from 2GHz (IF part of the receiver architecture) up to the whole RF bandwidth (in this case 15GHz). This means that a solution providing remote back-ends needs fiber optic (FO) links able to handle these orders of magnitude. To date a bandwidth of the order of ten GHz can be handled only with analog and very expensive FO systems. Instead, for a bandwidth of 2GHz Tx/Rx analog systems are available at a price of 1-1.5Keuro in quantities. A digital converter able to sample at 4Gsample/s is becoming available so also digital system links can be taken into account in the near future.
In this landscape at least three difficulties arises:

a) the need of a big amount of FO links due to both dense multifeed scheme and double architecture receiver (IF and RF signals). If N is the number of beams in the dense Mfeed, the total amount T of RF+IF signals should be 4*N, i.e. many tens of FO transmitter/receiver pairs. They have to be power supplied, the transmitters stocked in the receiver box or room (not always receiver boxes could be large enough to accomodate them) and got at a price higher than 4000÷6000*N euro (about 250000 euro for 50 beams receiver!)

b) the commercial available analog FO links, 2GHz wide, can slightly affect the dynamic range of the radioastronomical receiver and can show high noise figure.

c) the problem of sending 15GHz bandwidths, and much more in view of a multifeed in the band of 3mm of wavelength, still remains

8.2 Fiber optic links for remoting signals

Studies and tests on prototypes have been done by the Institute staff in the framework of the FARADAY and other projects. Results were reported in FARADAY Annual Reports [1] and [2] in which subsequent releases of the component reported in Fig. 8.2.1, coming from Andrew Co., were characterized. In figure 8.2.2 a summary of the salient parameters relative to a Tx/Rx link are reported, while in fig. 8.2.3 and 8.2.4 performances in term of variations of gain and phase with respect to temperature are shown.

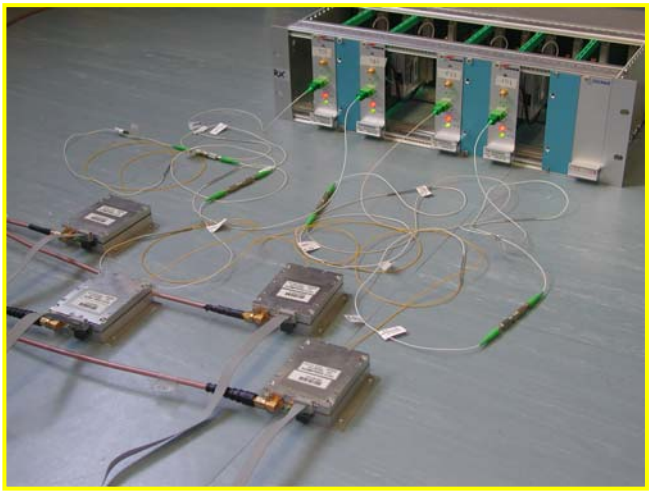

Fig. 8.2.1

Measurements 100MHz – 2200MHz	
Gain	*> 3.5 dB*
Input Return Loss	*> 15 dB*
Output Return Loss	*> 12 dB*
Input IP3	*> 29 dBm*
Noise Figure	*< 41 dB*
Relative Gain Stability	*< 1 dB*
Relative Phase Stability	*< 1°*

Fig. 8.2.2

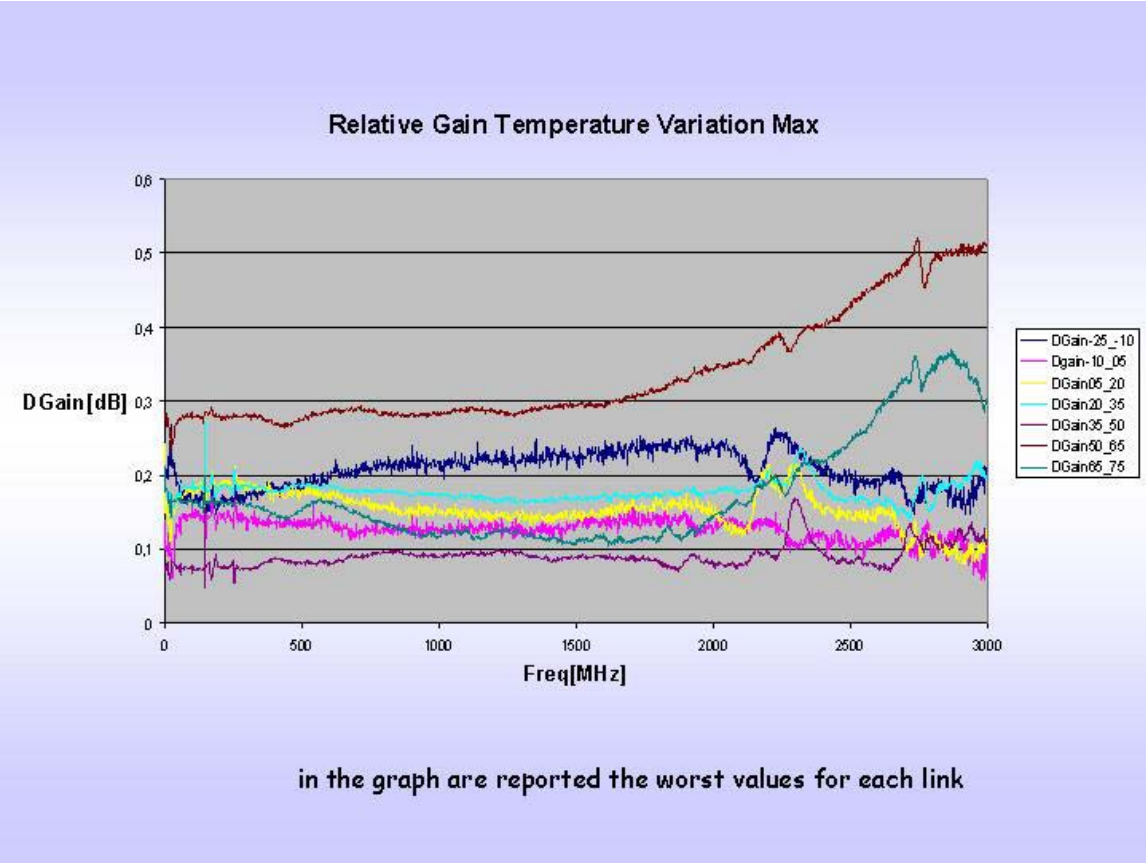

Fig. 8.2.3

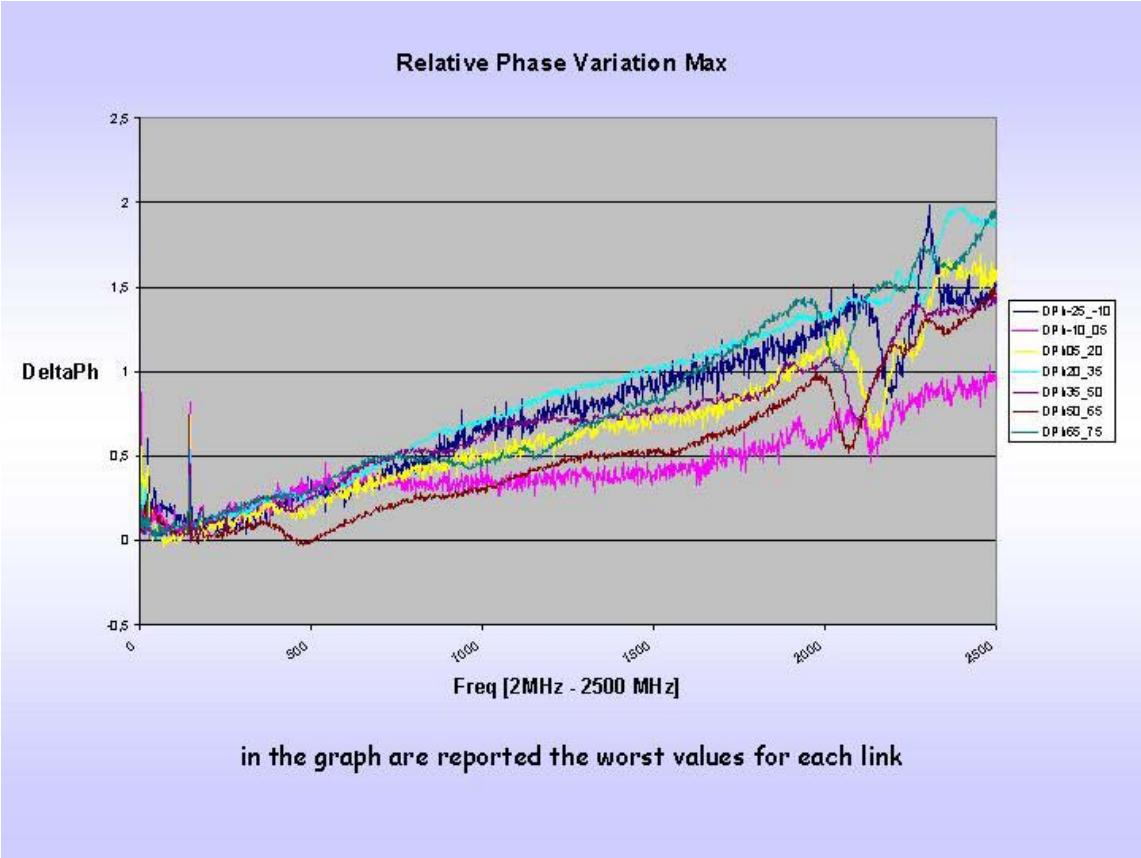

Fig. 8.2.4

Another component showing better performance in terms of noise figure, because it uses a preamplifier before the laser diode, but worst performance in term of spurious free dynamic range, a value less than 15dB with respect to the Andrew link, may be various Miteq products, available both up to 3 and 11GHz of bandwidth.

In any case the principal problem in using multifeed system is the necessity of a huge amount of FO links due to the related cost. The figure of cost reported above are made already taking into account the purchasing of some tens of links.
In view of this an alternative solution is try to locate as much back-ends as possibile on the antenna near the receivers. There is an exception in VLBI observations at the moment, because the Mark5 system of data storage, hard disk packages, have to be changed regularly during the observation so thay cannot be remotized, but this is not a problem because this kind of observation uses only a single feed-two channels receiver thus only a couple of FO links are needed.

REFERENCES

1. FARADAY Annual Reports 2002, 2003, 2004 Subproject 2
2. Montebugnoli S., Boschi M., Perini F., Faccin P., Brunori G., Pirazzini E.
"Large antenna array remoting using radio-over fiber techniques for radio astronomical application" Microwave and Optical Technology Letters vol. 46, no.1 July 2005